Acta Pharmaceutica Sinica B 2024;14(8):3543−3560

Chinese Pharmaceutical Association
Institute of Materia Medica, Chinese Academy of Medical Sciences

Acta Pharmaceutica Sinica B

www.elsevier.com/locate/apsb
www.sciencedirect.com

ORIGINAL ARTICLE

Ailanthone ameliorates pulmonary fibrosis by suppressing JUN-dependent MEOX1 activation

Lixin Zhao[†], Yuguang Zhu[†], Hua Tao[†], Xiying Chen, Feng Yin, Yingyi Zhang, Jianfeng Qin, Yongyin Huang, Bikun Cai, Yonghao Lin, Jiaxiang Wu, Yu Zhang, Lu Liang, Ao Shen[*], Xi-Yong Yu[*]

The Fifth Affiliated Hospital, Guangzhou Municipal and Guangdong Provincial Key Laboratory of Molecular Target and Clinical Pharmacology, NMPA & State Key Laboratory, School of Pharmaceutical Sciences, Guangzhou Medical University, Guangzhou 511436, China

Received 12 January 2024; received in revised form 1 April 2024; accepted 10 April 2024

KEY WORDS

Ailanthone;
MEOX1;
Pulmonary fibrosis;
JUN;
TGF-β1;
High-throughput screening;
Natural product

Abstract Pulmonary fibrosis poses a significant health threat with very limited therapeutic options available. In this study, we reported the enhanced expression of mesenchymal homobox 1 (MEOX1) in pulmonary fibrosis patients, especially in their fibroblasts and endothelial cells, and confirmed MEOX1 as a central orchestrator in the activation of profibrotic genes. By high-throughput screening, we identified Ailanthone (AIL) from a natural compound library as the first small molecule capable of directly targeting and suppressing MEOX1. AIL demonstrated the ability to inhibit both the activation of fibroblasts and endothelial-to-mesenchymal transition of endothelial cells when challenged by transforming growth factor-β1 (TGF-β1). In an animal model of bleomycin-induced pulmonary fibrosis, AIL effectively mitigated the fibrotic process and restored respiratory functions. Mechanistically, AIL acted as a suppressor of MEOX1 by disrupting the interaction between the transcription factor JUN and the promoter of MEOX1, thereby inhibiting MEOX1 expression and activity. In summary, our findings pinpointed MEOX1 as a cell-specific and clinically translatable target in fibrosis. Moreover, we demonstrated the potent anti-fibrotic effect of AIL in pulmonary fibrosis, specifically through the suppression of JUN-dependent MEOX1 activation.

*Corresponding authors.
E-mail addresses: shenao@gzhmu.edu.cn (Ao Shen), yuxycn@gzhmu.edu.cn (Xi-Yong Yu).
[†]These authors made equal contributions to this work.
Peer review under the responsibility of Chinese Pharmaceutical Association and Institute of Materia Medica, Chinese Academy of Medical Sciences.

https://doi.org/10.1016/j.apsb.2024.04.013

1. Introduction

Fibrosis is a common response to chronic or repetitive injury and stress affecting various organs and tissues such as the lungs, heart, kidneys, liver, skin, and joints[1]. Pathological fibrosis contributes to over one-third of natural deaths globally, resulting from the progressive loss of organ functions[2]. Among these fibrotic conditions, pulmonary fibrosis, especially in its idiopathic form (idiopathic pulmonary fibrosis, IPF), is a devastating disease with a lethal progression to respiratory failure[3]. Currently, pirfenidone and nintedanib are the only approved small molecule treatments for IPF[4]. However, they offer only partial relief from lung function decline and are associated with significant side effects[5–7]. Consequently, despite advancements in understanding fibrosis pathobiology, there is an urgent need for new anti-fibrotic small molecules for IPF and other fibrotic diseases.

Among various cell types in the lungs, fibroblasts, particularly in their activated form (myofibroblasts) play a central role in pulmonary fibrosis development[8]. Their activation, triggered by injury or stress, leads to the excessive accumulation of fibrillar, collagen-rich extracellular matrix (ECM), resulting in alveolar wall thickening and reduced lung elasticity. Besides resident fibroblasts, myofibroblasts can also derive from other cell types like epithelial and endothelial cells, which, under normal circumstances, have crucial secretory and regenerative roles in maintaining lung homeostasis[9,10]. Dysfunctions in these cells usually develop a profibrotic phenotype and contribute to IPF, making the inhibition of aberrant proliferation, activation, or transition of aforementioned cells a promising therapeutic strategy[11].

Injury or stress stimulates the release and activation of transforming growth factor-β1 (TGF-β1). It has been widely accepted that excessive TGF-β1 is a final common pathway in fibrotic diseases[12]. Persistent activation of TGF-β1/SMAD signaling drives multiple downstream pathways promoting fibroblast activation and transitions such as epithelial-mesenchymal transition (EMT) and endothelial-mesenchymal transition (EndMT) for epithelial and endothelial cells, respectively[13–15]. Strategies directly interfering with TGF-β1 or other cytokines boosted after TGF-β1 stimulation have been investigated for fibrotic diseases, yet none have successfully reached clinical application, primarily due to broad side effects associated with the multifunctional nature of these cytokines, crucial for maintaining tissue homeostasis[16].

Multiple studies have demonstrated the efficacy of BET inhibitors, such as JQ-1, in reducing fibrosis in various organs, including the heart[17,18], lungs[19,20] and liver[21]. A recent study revealed that during heart disease JQ-1 exerts its anti-fibrotic effect by inhibiting the expression of a transcription factor mesenchymal homobox 1 (MEOX1)[22]. MEOX1, a direct target of TGF-β1/SMAD, further governs the upregulation of broad fibrotic genes[22]. These findings not only elucidate the anti-fibrosis mechanism of BET inhibitors but also uncover how MEOX1 connects TGF-β1 with downstream profibrotic effectors. Thus, MEOX1 represents a clinically translatable target for fibrosis. Currently, no pharmaceutical solutions directly targeting MEOX1 have been developed[23].

In this study, we reported the elevated expression of MEOX1 in IPF patients specifically in their endothelial cells and fibroblasts, highlighting its pivotal role in pulmonary fibrosis. Additionally, we for the first time identified a small molecule Ailanthone (AIL) as a potent suppressor of MEOX1 through high-throughput screening (HTS) based on molecular pharmacological phenotypes. AIL effectively inhibited the proliferation, migration, and activation of lung fibroblasts and EndMT of endothelial cells when challenged by TGF-β1. In an animal model of bleomycin-induced pulmonary fibrosis, AIL effectively mitigated the fibrotic process and restored respiratory functions. Utilizing various chemical biology approaches, we mechanistically uncovered that MEOX1 orchestrates the activation of profibrotic genes and AIL disrupts the interaction between the transcription factor JUN and the promoter of *MEOX1* gene, thereby inhibiting MEOX1 activity, ultimately leading to the reductions in profibrotic genes and pulmonary fibrosis.

Taken together, our findings confirm MEOX1 as a cell-specific and clinically translatable target for pulmonary fibrosis and highlight Ailanthone as the first small molecule capable of directly targeting and suppressing MEOX1 activity. These results suggest that AIL might serve as a novel anti-fibrotic small molecule for IPF and other fibrotic diseases.

2. Material and methods

2.1. Reagents

Natural compound library (cat# L6000), Ailanthone (cat# TQ0209) and JQ-1 (cat# T5443) were obtained from TargetMol Chemicals (Boston, MA, USA). Anti-MEOX1 antibody (cat# sc-398845) was purchased from Santa Cruz Biotechnology (Santa Cruz, CA, USA). Antibodies against JUN (cat# ab32137), fibronectin (cat# ab45688), α-SMA (cat# ab124964), collagen I (cat# ab270993) and Alexa Fluor 488 and 594 conjugated secondary antibodies (cat# ab150077, ab150116) were purchased from Abcam (Cambridge, UK). Antibodies against α-tubulin (cat# 2144S), GAPDH (cat# 2118S), CD31 (cat# 77699T) and VE-cadherin (cat# 2158S) were obtained from Cell Signaling Technology (Boston, MA, USA). Recombinant human TGF-β1 (cat# 100-21) was purchased from PeproTech (Rocky Hill, CT, USA). Oligonucleotides used in this study for PCR and RNAi are listed in Supporting Information Table S1.

2.2. Plasmids

A DNA fragment containing human *MEOX1* promoter P0 region (−1000 to +359) was synthesized by Tsingke Biotechnology (Beijing, China) and cloned on pGL3-basic vector (Promega, Madison, WI, USA), denoted as pMEOX1-P0. Then the proximal (−206 to −33), P1 (1 to 359), P2 (−500 to −1) and P3 (−1000 to −1) regions of *MEOX1* promoter were amplified by PrimeSTAR Max DNA polymerase (Takara Bio, Japan) using pMEOX1-P0 as template and cloned on pGL3-basic vector, denoted as pMEOX1-proximal, -P1, -P2 and -P3, respectively. The P2 promoter was further subcloned to a dual-luciferase reporter vector (cat# P35419) obtained from

MiaoLingBio (Wuhan, China), in which Fluc was driven by P2 promoter and Rluc was driven by CMV promoter, denoted as P2-Fluc-Rluc. P2-ΔBS123-Fluc-Rluc, P2-ΔBS1-Fluc-Rluc, P2-ΔBS2-Fluc-Rluc, and P2-ΔBS3-Fluc-Rluc, in which either one or all three potential JUN binding sites were removed from P2-Fluc-Rluc, were synthesized by IGE Biotechnology (Guangzhou, China). The JUN overexpression plasmid pCDNA3.1-FLAG-JUN (cat# P11163) was obtained from MiaoLingBio (Wuhan, China). All plasmids used in this study were verified by both restriction digestion profile and DNA sequencing.

2.3. Cell culture and treatment

HeLa and MRC-5 cell lines were obtained from Procell (Wuhan, China). HPMECs were obtained from BNCC (Beijing, China). Cells were authenticated by STR profiling and free from mycoplasma contamination. MRC-5 cells were cultured in MEM plus NEAA medium (Procell, cat# PM150410) supplemented with 10% FBS (ExCell Bio) and 1% Penicillin−Streptomycin (Gibco, cat# 15140122) at 37 °C in an atmosphere of 5% CO_2. HPMECs were maintained in Endothelial Cell Medium (ScienCell, cat# 1001) containing 5% FBS, 1% ECGS (Corning, cat# 356006) and 1% Penicillin−Streptomycin. Primary mouse lung fibroblasts (PMLFs) were extracted from the lung tissues of 3-day-old mice according to the previous report[24]. For functional evaluation of MEOX1 in lung fibroblasts and endothelial cells, MRC-5 and HPMECs were infected with MEOX1-overexpressing lentivirus or transfected with si-*MEOX1* for 48 h, and then collected for qRT-PCR assay. For phenotypic detection of fibroblasts and endothelial cells, MRC-5, PMLFs and HPMECs were treated with or without TGF-β1 (5 ng/mL) followed by treatment with the indicated concentrations of AIL for 24 or 48 h before being collected for further analysis.

2.4. Luciferase assay

For the assay of identifying *MEOX1* promoter regions, HeLa cells were transfected with 500 ng of the indicated luciferase reporter vector (pMEOX1-P0, -Proximal, -P1, -P2 or -P3) and 25 ng of pRL-TK using the Lipofectamine 3000 (Thermo Fisher Scientific, CA, USA). The luciferase activity was measured after 48 h transfection.

For the HTS assay, HeLa cells were transfected with 20 μg P2-Fluc-Rluc in 10 cm dishes. At 24 h post-transfection, the cells were reseeded to 96 well plates for another 12 h. Compounds from the natural product library were then added into the plates for another 24 h with a final concentration of 10 μmol/L and then the luciferase activity was measured.

For the assay of determining AIL effect, after 24 h of transfection with P2-Fluc-Rluc, the cells were further treated with indicated concentration of AIL for another 24 h and then the luciferase activity was measured. Luciferase activities were measured by the dual-luciferase reporter assay system (Yeasen, cat# 11402ES60) according to the manufacturer's instructions. The ratio between firefly luciferase and renilla luciferase was calculated and normalized to untreated controls. Data were processed using Excel and Graphpad Prism 8.

2.5. Immunofluorescence staining

MRC-5 or HPMECs cells were seeded in a 96-well glass-bottom cell culture plates. After 24 h, cells were treated with PBS or TGF-β1 (5 ng/mL), and 0.1% DMSO or varying concentration of AIL were added for 24 h. Subsequently, the cells were fixed with 4% paraformaldehyde, permeabilized, and blocked. Cells were then incubated with one of the primary antibodies (1:200 dilution, anti-MEOX1, Fibronectin, α-SMA, Collagen I, CD31 or VE-cadherin) at 4 °C overnight, followed by Alexa Fluor-conjugated secondary antibodies (1:500 dilution) for 1 h at room temperature. After incubation with DAPI (Beyotime, cat# C1006) for 10 min at room temperature and washing three times, cells were imaged. Three independent batches of cells were tested, and each condition was imaged and analyzed in triplicate wells using CellInsight CX7 LZR (Thermo Scientific, CA, USA).

2.6. Animals

Animal studies were approved by the Institutional Animal Care and Use Committee of Guangzhou Medical University (Protocol 3001721) and performed in compliance with NIH guidelines for the care and use of laboratory animals. Male C57BL/6 mice aged 6−8 weeks (18−22 g) were obtained from SPF biotechnology (Beijing, China) and maintained in a pathogen-free facility. Animal sample size was estimated by a power calculation based on variability from a pilot study in the lab[25]. Mice were randomly divided into five groups: the normal control group (NC, $n = 18$), the AIL-treated group (AIL, $n = 18$), the BLM-treated group (BLM, $n = 25$), the BLM with additional AIL treatment group (BLM + AIL, $n = 20$) and the BLM with additional JQ-1 treatment group (BLM + JQ-1, $n = 20$). At Day 0, pulmonary fibrosis was induced by an intratracheal administration of bleomycin (3 mg/kg) under anesthesia. After BLM administration, animals were kept under normoxic conditions and each group was treated with AIL (5 mg/kg), JQ-1 (5 mg/kg), or an equal volume of saline by intraperitoneal injection every other day. On Day 3, ten mice in each group were randomly picked and sacrificed, bronchoalveolar lavage fluid of four mice and lung tissues of six mice were collected separately and used for further analysis. On Day 21, six mice in each group were randomly picked and their respiratory functions were evaluated by whole-body plethysmography (WBP, Buxco FinePointe), and then all remaining mice were sacrificed and tissues were collected for further analysis.

2.7. Quantitative real-time PCR

Total RNA from PMLFs, MRC-5, HPMECs and HeLa cells was individually extracted using RNA extraction kit (EZ Bioscience, cat# EZB-RN001-plus) and synthesized to cDNA by Hifair II 1st strand cDNA synthesis SuperMix (Yeasen, cat# 11123ES60). The TRIzol reagent was used to extract total RNA from lung tissues. The quantitative real-time PCR (qRT-PCR) analysis was performed on LightCycler 480 II system (Roche, Switzerland) using Hieff qPCR SYBR Green Master Mix (Yeasen, cat# 11201ES08). Relative expression levels were calculated and normalized to GAPDH or β-actin gene using the $2^{-\Delta\Delta Ct}$ method.

2.8. Western blot

Cells and tissues were lysed in RIPA buffer with protease inhibitors (Beyotime, Shanghai, China), and protein concentrations were determined using the BCA protein assay kit (Yeasen, cat# 20201ES76). Samples with equal amounts of total protein were

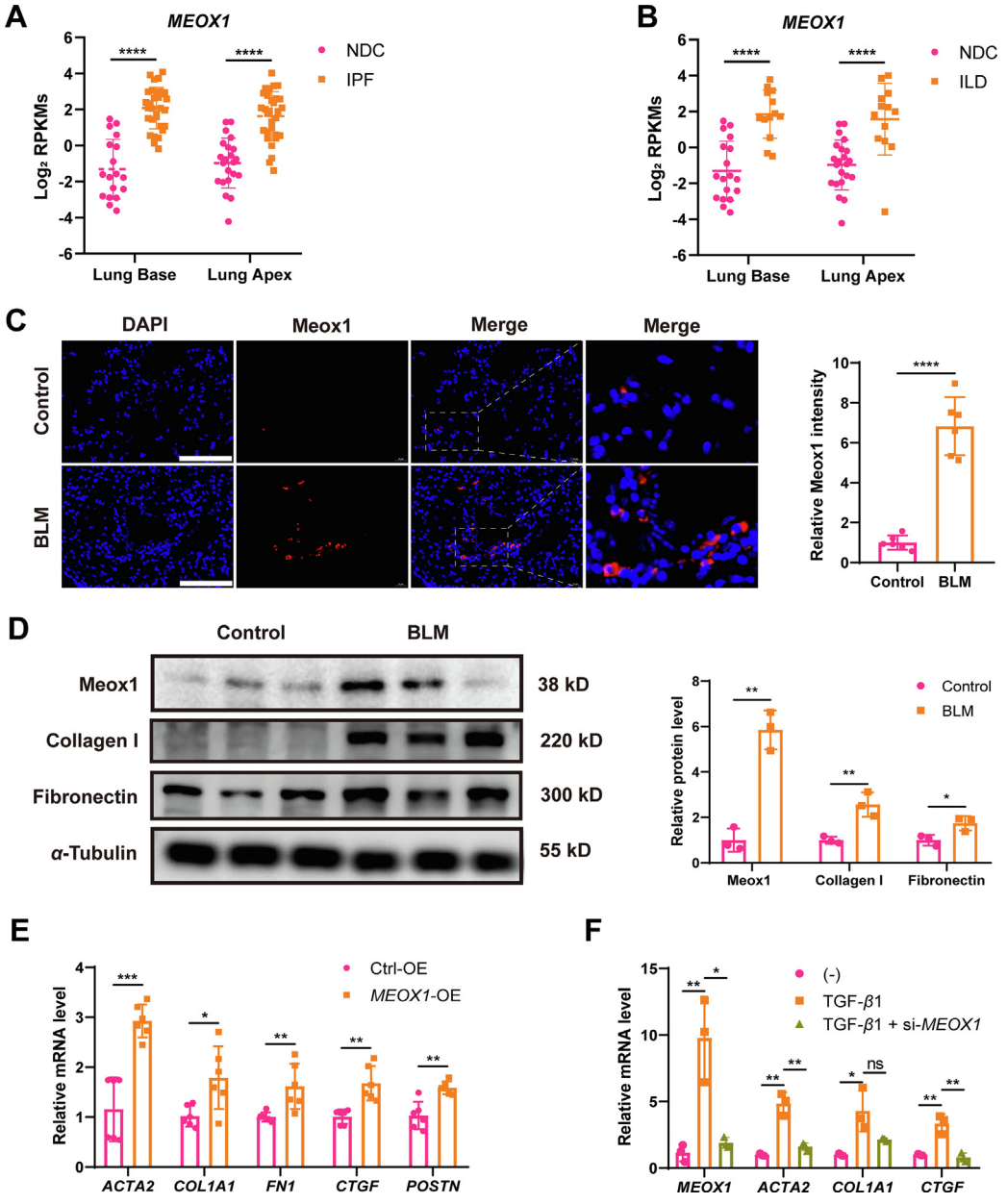

Figure 1 MEOX1 expression was significantly upregulated during pulmonary fibrosis. (A−B) *MEOX1* expression in lung tissues from non-diseased control (NDC) donors, idiopathic pulmonary fibrosis (IPF) patients and interstitial lung disease (ILD) patients were compared by RNA-seq (GSE213001). (C) Representative immunofluorescence images of lung tissue sections from normal and BLM-induced mice showing Meox1 expression, scale bars 100 μm, $n = 6$. The fluorescence intensity was quantified by ImageJ software. (D) The expressions of Meox1 and fibrotic markers Collagen I and Fibronectin in lung tissues from normal and BLM-induced mice were analyzed by Western blotting and quantified, $n = 3$. (E) The relative mRNA levels of *ACTA2*, *COL1A1*, *FN1*, *CTGF* and *POSTN* in MRC-5 cells infected with lentivirus overexpressing *MEOX1* or control vector, $n = 6$. (F) The relative mRNA levels of *MEOX1*, *ACTA2*, *COL1A1*, and *CTGF* in MRC-5 cells transfected with siRNA knocking down *MEOX1* with or without TGF-β1 induction, $n = 3$. Data are presented as mean ± SD; $^{*}P < 0.05$, $^{**}P < 0.01$, $^{***}P < 0.001$, $^{****}P < 0.0001$ by two-tailed Student's *t*-test.

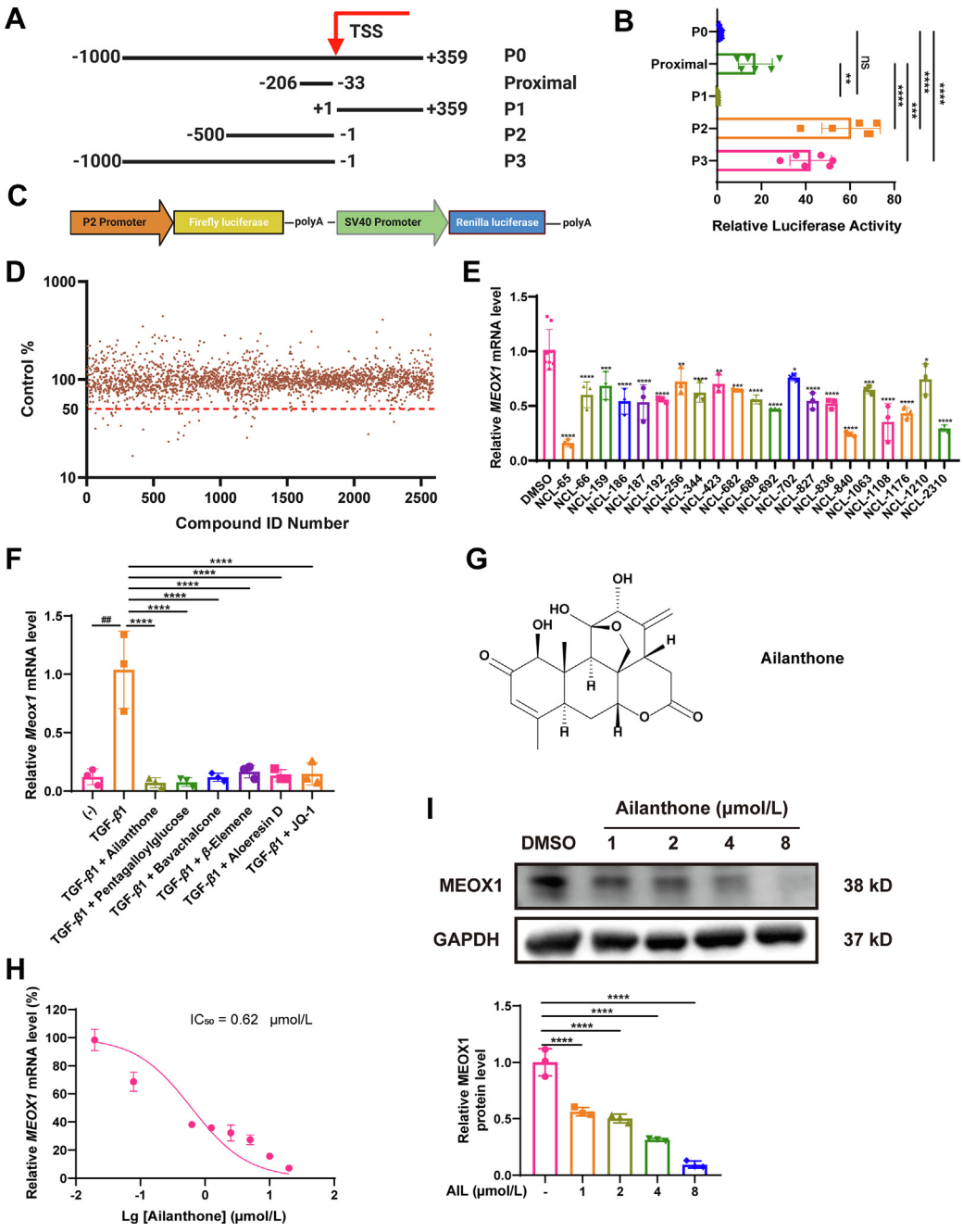

Figure 2 Ailanthone was a potent MEOX1 suppressor. (A) Sketch of the gene structure of human MEOX1. Transcriptional start site (TSS) and promoter regions with different length were shown. (B) HeLa cells transfected with reporters containing various length of *MEOX1* promoter regions were measured by luciferase activities. (C) Schematic of the MEOX1 reporter construct used in high-throughput screening. (D) Summary of MEOX1 reporter activities evaluating all natural compounds screened in this study against MEOX1 P2 promoter. The ratio between firefly luciferase and renal luciferase was calculated and normalized to DMSO controls. (E) Changes of *MEOX1* expression by hit compounds in HeLa cells. The mRNA level of *MEOX1* in all groups was normalized to DMSO group. (F) The mRNA level of *Meox1* was determined in primary mouse lung fibroblasts (PMLFs) incubated with hit compounds (10 μmol/L) after TGF-β1 (5 ng/mL) stimulation. (G) Chemical structures of AIL. (H) The expression of *MEOX1* was measured in the presence of varying concentrations of AIL by qRT-PCR and IC_{50} was determined, $n = 3$. (I) The protein level of MEOX1 in HeLa cells treated with varying concentrations of AIL for 24 h was analyzed by Western blotting and quantified, $n = 3$. Data are presented as mean ± SD; $^{\#\#}P < 0.01$ by two-tailed Student's *t*-test; $^{*}P < 0.05$, $^{**}P < 0.01$, $^{***}P < 0.001$, $^{****}P < 0.0001$ by one-way ANOVA followed by Tukey's *post hoc* test between indicated groups.

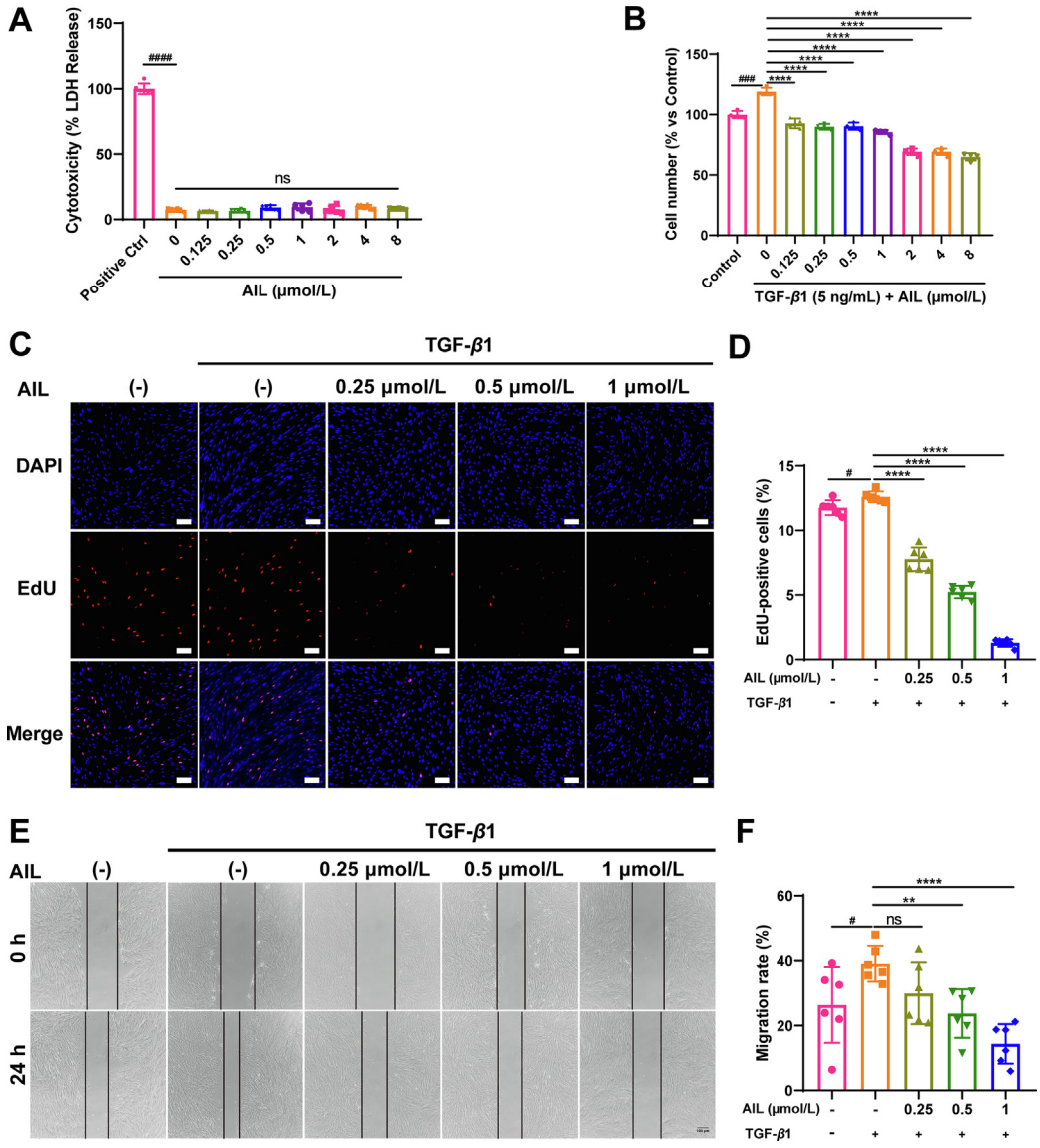

Figure 3 Ailanthone suppressed proliferation and migration of pulmonary fibroblasts under TGF-β1 stimulation. (A) MRC-5 cells were incubated with various concentrations of AIL for 24 h and then harvested for LDH release assay, $n = 6$. (B) The concentration-dependent inhibitory effect of AIL on MRC-5 cells under TGF-β1 stimulation was determined by CCK-8, $n = 4$. (C) Representative images of EdU assay on AIL-treated MRC-5 cells, cell nuclei stained with DAPI are shown in blue, and EdU-positive cell nuclei are shown in red, Scale bars: 100 μm. (D) Statistics of the EDU-positive ratio was analyzed with Thermo Scientific CellInsight CX7 LZR software. (E) Migration of AIL-treated MRC-5 cells were detected by wound healing assay, Scale bars: 100 μm. (F) Statistics of the wound area from (E); $n = 6$. Data are presented as mean ± SD; $^{\#}P < 0.05$, $^{\#\#\#}P < 0.001$, $^{\#\#\#\#}P < 0.0001$ by two-tailed Student's *t*-test; $^{**}P < 0.01$, $^{****}P < 0.0001$ by one-way ANOVA followed by Tukey's *post hoc* test between indicated groups.

separated on precast PAGE gels (Beyotime, cat# P0468S) and transferred to PVDF membrane (Pall Life Sciences, Ann Arbor, MI, USA). Primary antibodies against MEOX1 (1:1000), FN1 (1:1000), α-SMA (1:1000), CD31 (1:1000) and collagen I (1:1000) were incubated with PVDF membranes at 4 °C overnight, α-tubulin (1:2000) or GAPDH (1:1000) served as a loading control. The membranes were probed with HRP-conjugated secondary antibodies (1:5000) for 1.5 h at room temperature. The western lightning plus chemiluminescence reagent (PerkinElmer, Shelton, USA) was used to visualize the protein of interest using Amersham imager AI600 (GE Healthcare) and quantitated by ImageJ software.

2.9. *Histopathology and immunofluorescence staining*

Histopathology staining was performed by Servicebio (Wuhan, China). Briefly, lung tissues were fixed in 4% paraformaldehyde and embedded in paraffin to make 5-μm tissue sections. Hematoxylin and eosin (H&E) and Masson's trichrome staining were performed according to the standard protocol, and images were obtained by Aperio CS2 digital slide scanner (Leica Biosystems Imaging, Germany). The histologic severity for fibrosis was quantified by Ashcroft scoring system as previously described[26]. In brief, the degree of fibrosis in lung specimens ranges from grade 0 (normal lung) to grade 8 (fibrous

obliteration) was evaluated by an independent analyst blinded to group allocation. The average score of each microscopic field in the entire lung slide was used as the fibrosis score. Collagen volume fraction (CVF) of lung tissues was calculated by ImageJ software. For immunofluorescence staining assays, the tissue sections were deparaffinated in 3 changes of xylene, 10 min each, then dehydrate in 3 changes of pure ethanol for 5 min each, wash in distilled water. After incubation with 3% hydrogen peroxide, the sections were heated to repair antigen and cooled to room temperature. The sections were blocked with 3% BSA for 30 min, followed by incubation with the indicated antibodies at 4 °C overnight. The next day, sections were shaken on the decoloring shaker for 3 times, 5 min each time. Then the sections were incubated with secondary antibody at room temperature for 50 min in the dark and followed with DAPI (Beyotime, cat# C1006) for 10 min at room temperature and washed for three times. Images were collected by a Pannoramic Scan II digital slide scanner (3DHISTECH, Hungary).

2.10. Hydroxyproline determination

The collagen content in mouse lung tissues was assessed according to the instruction of the hydroxyproline assay kit (Solarbio, Beijing, China, BC0255). In brief, the right lung of each mouse was precisely weighed and cut into very small pieces and digested 4−6 h at 110 °C within digestion buffer. After adjusting pH, the supernatant was obtained by centrifugation at 16,000 rpm for 20 min at 25 °C. After that, hydroxyproline concentration in the homogenate was determined at 550 nm absorbance by a Synergy LX microplate reader (BioTek, USA).

2.11. Wound healing assay

MRC-5 or HPMECs were cultured in 6-well plates till 90% confluent. The cell monolayer was scratched by the tip of 20 μL micropipette and cultured under standard culture conditions. The cells then were treated with TGF-β1 and indicated concentration of AIL, and the images were captured with Echo-lab Revolve imaging system (ECHO, San Diego, USA) at 0, 12/24 h. Migration rate was calculated by ImageJ software.

2.12. Transwell assay

Transwell polycarbonate membrane inserts (pore size 8 μm) were bought from Corning (Corning, NY, USA). Briefly, MRC-5 or HPMECs cells were suspended in serum-free medium and seeded into the upper chamber of Transwell at the density of 2×10^4 cells per well, and the lower chamber were filled with 600 μL complete medium with serum. After incubating for 24 h with indicated treatment, the cells adhered to the lower surface of the membrane were fixed using paraformaldehyde and stained with 0.1% crystal violet. The migrated cells were captured by a microscope and counted using ImageJ software.

2.13. Cell monolayer permeability

The HPMECs treated with the indicated concentrations of AIL with or without TGF-β1 (5 ng/mL) were growing as monolayers on fibronectin-coated transwell plates for 48 h. 5 mg/mL FITC-albumin (Solarbio, cat# SF063) was added to the upper chamber of the transwell, and incubated in 37 °C for 1 h. Culture media from the lower chambers were collected for FITC fluorescent intensity analysis using a LB943 Mithras2 plate reader (Berthold Technologies, Germany) at excitation 494 nm.

2.14. EdU fluorescence staining

A Cell-Light EdU Apollo 594 *in vitro* kit (RiboBio, Guangzhou, China) was used to detect cell proliferation. MRC-5 cells were cultured in 96-well imaging plates. 24 h later, cells were stimulated with TGF-β1 (5 ng/mL) and indicated concentration of AIL for 24 h, the EdU assay was carried out according to the manufacturer's protocol.

2.15. RNA seq

MRC-5 cells cultured in 100 mm plates were divided into 3 groups: control group (no treatment), TGF-β1 group (stimulated with 5 ng/mL TGF-β1), TGF-β1 + AIL group (stimulated with 5 ng/mL TGF-β1 and 1 μmol/L AIL). 24 h later, 3 plates per group were used for RNA sequencing (BioMarker, Beijing, China). In brief, the total RNA from each group was individually extracted according to the instruction manual of the TRIzol Reagent (Life technologies, CA, USA). RNA concentration and purity was measured using NanoDrop 2000 (Thermo Fisher Scientific, DE, USA). RNA integrity was assessed using the RNA Nano 6000 Assay Kit of the Agilent Bioanalyzer 2100 system (Agilent Technologies, CA, USA). A total amount of 1 μg RNA per sample was used as input material for the RNA sample preparations. Sequencing libraries were generated using Hieff NGS Ultima Dual-mode mRNA Library Prep Kit for Illumina (Yeasen, Shanghai, China) following manufacturer's recommendations and index codes were added to attribute sequences to each sample. The libraries were sequenced on an Illumina NovaSeq platform to generate 150 bp paired-end reads, according to the manufacturer's instructions. The raw reads were further processed with a bioinformatics pipeline tool BMKCloud (www.biocloud.net).

2.16. Chromatin immunoprecipitation (ChIP) assay

The ChIP assay was performed using BeyoChIP chromatin immunoprecipitation assay kit (Beyotime, cat# P2080S) following the manufacturer's instructions. Briefly, HeLa cells were cross-linked with 1% formaldehyde solution. Nucleoprotein complexes were incubated with either the anti-JUN antibody or an isotope-matched antibody (mouse IgG) pre-coupled with Protein A/G magnetic beads at 4 °C overnight. After that, DNA was purified from magnetic beads and eluted with DNA elution buffer. Quantitative real-time PCR was carried out to verify the binding ability between JUN and the promoters of target genes. Three primer sets were designed to cover the potential binding sites for JUN on the *MEOX1* promoter. The primers were listed in Table S1. The amount of immunoprecipitated DNA was normalized to the input. ChIP-qPCR data was analyzed by $2^{-\Delta\Delta Ct}$ method.

2.17. Electrophoretic mobility shift assay (EMSA)

EMSA assays were conducted using a chemiluminescent EMSA kit (Beyotime, cat# GS009). The biotin-labeled AP-1 probe was purchased from Beyotime (cat# GS011B). The biotin-labeled DNA probes containing predicted JUN binding site (BS1: ATTCCTCACT, BS2: ATTAATCATC, and BS3: ATTTGTCACT) within MEOX1 P2 promoter and their unlabeled competitors (cold probes) which had the identical sequence as the labeled probes were synthesized by Tsingke Biotechnology. The details of probe

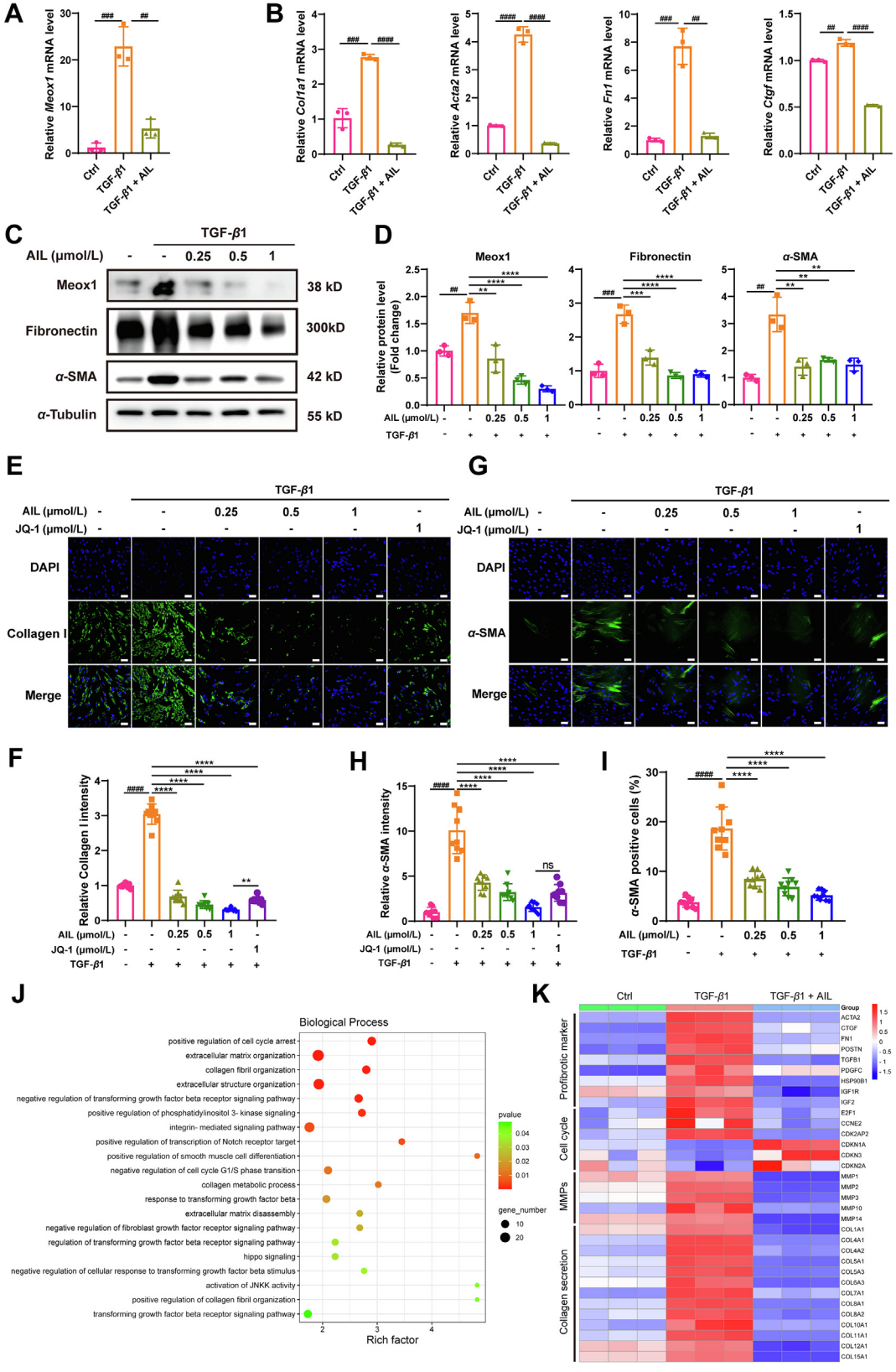

Figure 4 Ailanthone inhibited lung fibroblasts activation and fibrogenesis induced by TGF-β1. (A, B) PMLFs were stimulated with TGF-β1 (5 ng/mL) and treated with AIL (1 μmol/L) for 24 h. The relative mRNA levels of *Meox1*, *Col1a1*, *Acta2*, *Fn1* and *Ctgf* were measured by the qRT-PCR; $n = 3$. (C, D) PMLFs were stimulated with TGF-β1 (5 ng/mL) and treated with the indicated concentrations of AIL for 24 h. The

sequence are listed in Table S1. Reaction solutions contained EMSA/Gel-Shift binding buffer (Beyotime, cat# GS005), 2 μL of 5 mg/mL HeLa nuclear extract, different concentrations of AIL and ultra-pure water to a total volume of 9 μL. These solutions were incubated at room temperature for 10 min and then 1 μL of 0.2 μmol/L biotin-labeled probes with or without 100-fold molar excess of cold probes were added. The mixtures were then incubated for another 20 min at room temperature. For super-shift EMSA, Biotin-labeled DNA probe containing BS2 sequence was incubated with or without HeLa nuclear extracts, in the absence or presence of anti-JUN antibody or 100-fold molar excess of cold probe. Samples were electrophoresed on a 6% BeyoGel EMSA precast PAGE gel (Beyotime, cat# GS306S) and then transferred to nylon membranes, UV cross-linked, probed with streptavidin-HRP conjugate and incubated with the BeyoECL Moon working solution as the manufacturer's instructions. The results were detected by Amersham imager AI600 (GE Healthcare).

2.18. Molecular docking

The molecular docking study, including consensus SAR modeling, protein preparation, ligand preparation and docking, was conducted using MOE 2022 (Chemical Computing Group, Montreal, Canada). The crystal structure of JUN/FOS/DNA complex (PDB code: 1FOS) was load into MOE, the DNA sequence was substituted for ATTAATCATC (BS2) and prepared by adding missing atoms, removing solvent and taking energy minimization using QuickPrep module. The three dimensional structures of AIL was produced by minimizing energy and conformational search. According to JUN/FOS/BS2 complex interface, the best docking site was found through Site Finder function. AIL was then docked and the top 10 complexes were recorded and analyzed.

2.19. Cartoon development

Diagrams were created with BioRender.com.

2.20. Statistics and analysis

All experiments were repeated independently at least 3 times. Data collected were tested for normality using Shapiro−Wilk and Kolmogorov−Smirnov normality tests. All normally distributed data were presented as the mean ± standard deviation (SD), and analyzed by either two-tailed Student's *t*-test between two groups or one-way ANOVA followed by Tukey's *post hoc* test for three or more groups by Prism 8 (GraphPad Software, San Diego, CA, USA). $P < 0.05$ was defined as statistically significant.

2.21. Data availability

The data that support the findings of this study are present in the paper or the Supporting Information. Any additional information required for reanalysis is available from the corresponding authors upon reasonable request.

3. Results

3.1. MEOX1 was significantly upregulated in patients with pulmonary fibrosis and a mouse model of pulmonary fibrosis

To explore the potential role of MEOX1 in pulmonary fibrosis, first we conducted an analysis of RNA-seq data (GSE213001) in lung tissues from 14 non-diseased control (NDC) donors and 20 idiopathic pulmonary fibrosis (IPF) patients[27]. The expression of MEOX1 was significantly elevated in IPF lung tissue, both in the lung apex and the lung base (Fig. 1A). Considering that diffuse lung parenchyma and interstitial fibrosis are typical pathological features of interstitial lung disease (ILD), we also compared MEOX1 expression in lung tissues from 14 NDC donors and 13 ILD patients. Consistent with the findings in IPF lung tissues, MEOX1 was also markedly increased in ILD lung tissues (Fig. 1B). Bleomycin (BLM)-induced pulmonary fibrosis represents a widely used experimental model for studying human pulmonary fibrosis. As expected, immunofluorescence analysis of tissue sections revealed an upregulation in the expression of Meox1 in the lung tissues of BLM-induced mice (Fig. 1C). This finding was subsequently validated through Western blot analysis of the lung lysates (Fig. 1D).

We then overexpressed *MEOX1* in MRC-5 cells (human embryonic lung fibroblasts) and observed a notable upregulation of profibrotic genes such as α-smooth muscle actin (*ACTA2*), collagen I (*COL1A1*), fibronectin (*FN1*), connective tissue growth factor (*CTGF*) and periostin (*POSTN*), indicating MEOX1 as a significant driver of fibrosis (Fig. 1E). In line with *in vivo* results, endogenous MEOX1 expression also showed a significant increase when cells were stimulated with TGF-β1, along with profibrotic markers (Fig. 1F). More importantly, to assess the therapeutic potential of targeting MEOX1 in pulmonary fibrosis, we employed siRNA to knockdown *MEOX1* in TGF-β1-treated MRC-5 cells. The qRT-PCR results revealed a significant reduction in the expression of *ACTA2*, *COL1A1*, and *CTGF* upon *MEOX1*

relative protein levels of Meox1, α-SMA and Fibronectin were analyzed by Western blotting and quantified, $n = 3$. (E) Representative immunofluorescence images of MRC-5 cells stimulated with TGF-β1 (5 ng/mL) and treated with the indicated concentrations of AIL or JQ-1 for 24 h showing collagen I expression, Scale bars: 100 μm. (F) The relative fluorescence intensity of collagen I was analyzed with ImageJ software; $n = 9$. (G) Representative immunofluorescence images of MRC-5 cells stimulated with TGF-β1 (5 ng/mL) and treated with the indicated concentrations of AIL or JQ-1 for 24 h showing α-SMA expression, Scale bars: 100 μm. (H) The relative fluorescence intensity of α-SMA was analyzed with ImageJ software; $n = 9$. (I) The fibroblast-to-myofibroblast conversion ratio in (G) was analyzed with Thermo Scientific CellInsight CX7 LZR software by determining α-SMA-positive cells (myofibroblast) and DAPI-positive cells (total fibroblast). (J) Gene Ontology (GO) analysis of changed genes in MRC-5 cells stimulated with TGF-β1 (5 ng/mL) and treated with or without AIL (1 μmol/L) for 24 h. Log2fold-change > 1, padj < 0.05. (K) Heatmaps of profibrotic marker, cell-cycle, collagen secretion and matrix metalloproteinases (MMPs) related genes in control group, TGF-β1 group (5 ng/mL) and TGF-β1 group with AIL (1 μmol/L) treatment for 24 h. Data are presented as mean ± SD; $^{\#\#}P < 0.01$, $^{\#\#\#}P < 0.001$, $^{\#\#\#\#}P < 0.0001$ by two-tailed Student's *t*-test; $^{**}P < 0.01$, $^{***}P < 0.001$, $^{****}P < 0.0001$ by one-way ANOVA followed by Tukey's *post hoc* test between indicated groups.

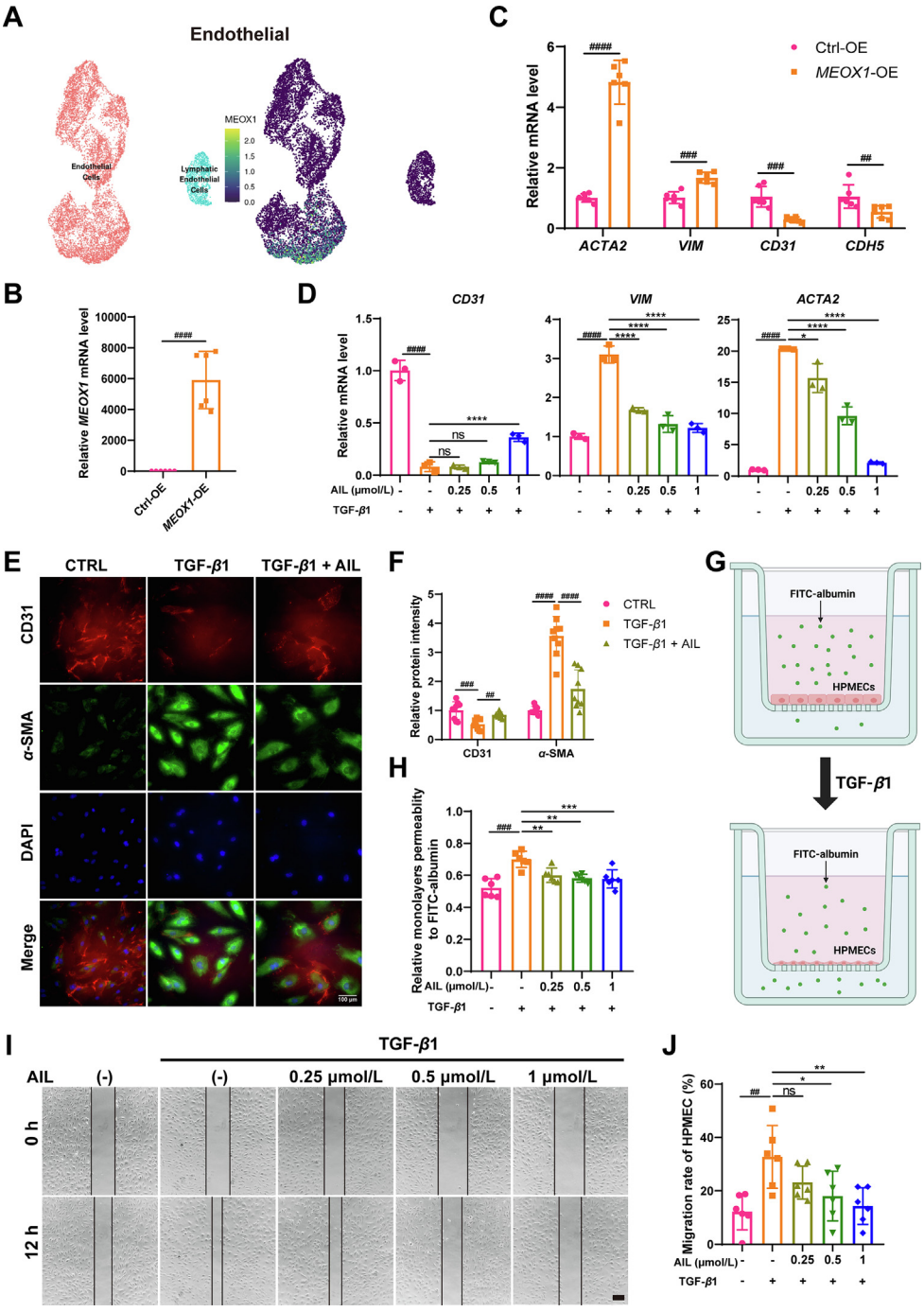

Figure 5 Ailanthone suppressed EndMT, barrier permeability and migration of endothelial cells under TGF-β1 stimulation. (A) UMAP representation of *MEOX1* expression in endothelial cells isolated from lungs of 20 pulmonary fibrosis patients and 10 normal donors (dataset GSE135893). (B, C) The relative mRNA levels of *MEOX1*, *ACTA2*, *VIM*, *CD31* and *CDH5* in HPMECs infected with lentivirus overexpressing *MEOX1* or control vector, $n = 6$. (D) The relative mRNA levels of EndMT markers *CD31*, *VIM* and *ACTA2* in HPMECs treated as indicated were measured by qRT-PCR; $n = 3$. (E) Immunofluorescence analysis for CD31 (red) and α-SMA (green) in HPMECs treated as indicated, Scale bars: 100 μm. (F) The relative fluorescence intensity of CD31 and α-SMA was analyzed with ImageJ software; $n = 9$. (G) Schematic of the permeability assay of HPMECs monolayers. (H) Permeability of HPMECs monolayers treated with TGF-β1 (5 ng/mL) and AIL as indicated was quantified based on fluorescence intensity of FITC in the culture media in the lower chambers; $n = 6$. (I) Wound healing assay was performed on HPMECs following treated with TGF-β1 (5 ng/mL) and AIL as indicated, representative images are shown, scale bars: 100 μm. (J) Quantification of the cell migration rate; $n = 6$. Data are presented as mean ± SD; $^{\#\#}P < 0.01$, $^{\#\#\#}P < 0.001$, $^{\#\#\#\#}P < 0.0001$ by two-tailed Student's *t*-test; $^{*}P < 0.05$, $^{**}P < 0.01$, $^{***}P < 0.001$, $^{****}P < 0.0001$ by one-way ANOVA followed by Tukey's *post hoc* test between indicated groups.

knockdown, thus confirming the potential of MEOX1 as a therapeutic target in pulmonary fibrosis (Fig. 1F).

3.2. *Natural compound screening identified ailanthone as a MEOX1 suppressor*

Transcription factors have traditionally been considered challenging to target due to structural complexities and the absence of well-defined binding pockets for small molecules[28]. To identify chemical compounds that can regulate the activity or expression of MEOX1, we decided to perform a cell-based HTS screening. First of all, we investigated the expression of MEOX1 in various human cell lines in the Human Protein Atlas database (www.proteinatlas.org). The results showed that the expression of MEOX1 in HeLa cells was the highest in all queried cell lines, promoting us to choose HeLa cells as the HTS cell line (Supporting Information Fig. S1A). Then, we functionally identified the human *MEOX1* gene promoter regions with high luciferase reporter sensitivity. The *MEOX1* proximal promoter (−236 to −33 bp from TSS) reported previously[29] and P0 promoter (−1000 to +359 bp) were cloned into pGL3-Basic reporter vector separately (Fig. 2A). Comparing with pGL3-Basic, the luciferase activities of HeLa cells transfected with either proximal promoter or P0 promoter increased by 1727% and 161%. Given that the proximal promoter and P0 promoter had such a distinct response, we further narrowed down P0 promoter into 3 fragments and found that P2 promoter (−500 to −1 bp) had the best activity among all fragments tested (Fig. 2B). Subsequently, we conducted a dual-luciferase reporter assay based on MEOX1 P2 promoter (Fig. 2C). The Z-factor of the dual-luciferase reporter assay was determined to be 0.60 (Fig. S1B), suggesting that it could be applied to screening on a larger scale. Finally, the HTS assay was subject to screen a natural compound library. A single dose at 10 μmol/L was tested in the primary screen and only the inhibition rate over 50% was selected for the second screening (Fig. 2D and Fig. S1C). In the second screening, we evaluated the inhibitory effect of individual compounds (10 μmol/L) on the expression of *MEOX1* in HeLa cells by qRT-PCR. The results showed that NCL-65 (Ailanthone), NCL-840 (1,2,3,4,6-*O*-pentagalloylglucose), MCL-1108 (Bavachalcone), NCL-1176 (*β*-Elemene) and NCL-2310 (Aloeresin D) reduced the expression of *MEOX1* by 60%, which were consistent with the results of the dual-luciferase assay (Fig. 2E).

Next, we assessed whether above compounds could reverse the upregulation of *Meox1* induced by TGF-*β*1 in PMLFs. As expected, ailanthone, 1,2,3,4,6-*O*-pentagalloylglucose, bavachalcone, *β*-elemene, and aloeresin D could serve as suppressors of *Meox1* expression (Fig. 2F, G and Fig. S1D). It is worth noting that ailanthone (AIL) inhibited *Meox1* by over 90% at 10 μmol/L, exhibiting the highest potency against *Meox1* among the tested compounds and also surpassing the performance of JQ-1. So we selected AIL for the dose-response curve determination. Eventually, we identified AIL as the best hit compound inhibited the mRNA expression of *MEOX1* with IC_{50} values of 0.62 μmol/L (Fig. 2H). In addition, AIL also suppressed the protein expression of MEOX1 in a dose-dependent manner (Fig. 2I).

3.3. *Ailanthone suppressed proliferation and migration of lung fibroblasts induced by TGF-β1*

In response to injury, the initial stage of tissue repair involves the proliferation and migration of activated fibroblasts, contributing to the development of pulmonary fibrosis[30]. To assess the impact of AIL on TGF-*β*1-induced fibroblast proliferation and migration, MRC-5 cells were cultured with or without TGF-*β*1 and varying doses of AIL for 24 h. LDH release assay indicated that AIL exhibited no cytotoxic effect on fibroblasts at concentrations below 10 μmol/L (Fig. 3A). The proliferation of MRC-5 cells, when assessed through CCK-8 assay, revealed a dose-dependent suppression of fibroblast proliferation by AIL in response to TGF-*β*1 activation (Fig. 3B). Consistently, in EdU incorporation assay a notable reduction in EdU-positive cells was observed with AIL treatment in a dose-dependent manner (Fig. 3C and D). Furthermore, the wound healing assay demonstrated that AIL dose-dependently decreased the migration rate of activated fibroblasts induced by TGF-*β*1 (Fig. 3E and F). Additionally, a transwell migration assay confirmed the concentration-dependent reduction in fibroblasts in the lower transwell chamber with AIL treatment (Supporting Information Fig. S2A and S2B). Taken together, these results indicate that AIL exhibited potent concentration-dependent inhibitory effects on the proliferation and migration of lung fibroblasts.

3.4. *Ailanthone inhibited lung fibroblasts activation and fibrogenesis induced by TGF-β1*

MEOX1 has been identified as a transcriptional switch from cardiac fibroblast to myofibroblast, and consistently, we observed an increase in MEOX1 expression in myofibroblasts within the lung. Therefore, we investigated the effect of AIL on pulmonary fibroblast activation and fibrogenesis. As shown by qRT-PCR, AIL could inhibit the TGF-*β*1-induced upregulation of *Meox1* (Fig. 4A), as well as suppress the mRNA expression levels of profibrotic genes such as *Col1a1*, *Acta2*, *Fn1*, and *Ctgf* (Fig. 4B). Similarly, Western blot analysis confirmed that AIL could dose-dependently reduce the protein expression levels of Meox1, *α*-SMA and Fibronectin induced by TGF-*β*1 (Fig. 4C and D). Immunofluorescence assays further validated that AIL suppressed the TGF-*β*1-induced expression of MEOX1 (Supporting Information Fig. S3A and S3B), as well as that of Collagen I and Fibronectin (Fig. 4E, F, Fig. S3C and S3D). Additionally, *α*-SMA, a hallmark of myofibroblasts, was upregulated under TGF-*β*1 stimulation, leading to an increased fibroblast-to-myofibroblast conversion ratio (as determined by *α*-SMA-positive cells). However, as expected, both the expression of *α*-SMA and the myofibroblast ratio were decreased in the AIL-treatment group (Fig. 4G−I).

To understand the underlying mechanisms of AIL in the inhibition of TGF-*β*1-induced fibroblasts activation, we performed RNA-seq of MRC-5 cells treated with DMSO, TGF-*β*1 alone, or TGF-*β*1 together with AIL. Gene Ontology (GO) analysis revealed that AIL led to a genome-wide change in biological processes related to fibroblast activation and ECM deposition, such as positive regulation of cell cycle arrest, ECM organization, collagen fibril organization, extracellular structure organization, and the TGF-*β* receptor signaling pathway (Fig. 4J). Heatmap analysis revealed that AIL intervention reversed the upregulation of profibrotic markers, cell-cycle-related genes, collagen secretion, and matrix metalloproteinases (MMPs) induced by TGF-*β*1 (Fig. 4K).

3.5. *Ailanthone suppressed EndMT, barrier permeability and migration of endothelial cells induced by TGF-β1*

Considering the heterogeneity of cells in the lungs, we performed the single-cell RNA sequencing (scRNA-seq) analysis

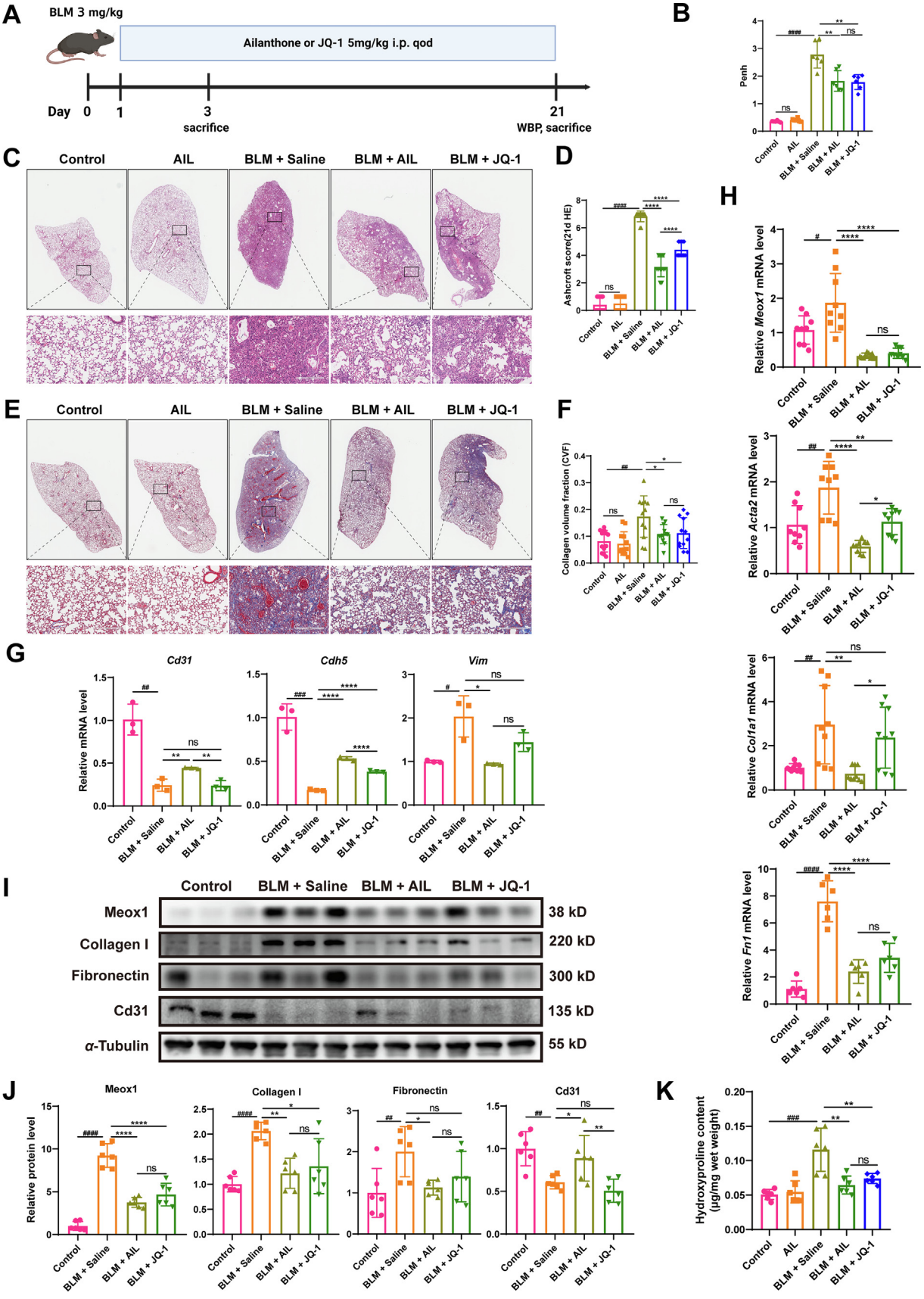
A
BLM 3 mg/kg
Ailanthone or JQ-1 5mg/kg i.p. qod
Day 0 1 3 21
sacrifice
WBP, sacrifice
B
Penh
C
Control
AIL
BLM + Saline
BLM + AIL
BLM + JQ-1
D
Ashcroft score(21d HE)
E
F
Collagen volume fraction (CVF)
G
Cd31
Cdh5
Vim
Relative mRNA level
H
Relative Meox1 mRNA level
Relative Acta2 mRNA level
Relative Col1a1 mRNA level
Relative Fn1 mRNA level
I
Meox1
Collagen I
Fibronectin
Cd31
α-Tubulin
38 kD
220 kD
300 kD
135 kD
55 kD
J
Relative protein level
K
Hydroxyproline content (μg/mg wet weight)

of cells isolated from the lungs of IPF patients and normal donors. The GSE135893 dataset[31] was analyzed by IPF Cell Atlas tools[32] (http://ipfcellatlas.com/). Based on relative similarity, four cell-type clusters were identified: epithelial, endothelial, mesenchymal and immune. We noticed that MEOX1 was predominantly expressed in endothelial cells (ECs) and fibroblasts, suggesting a cell-specific expression pattern, with notably higher expression in ECs than in fibroblasts (Fig. 5A and Supporting Information Fig. S4A–S4C). More importantly, *MEOX1* expression was further elevated in ECs and fibroblasts in ILD patients (Fig. S4D). Given the high expression of *MEOX1* in pulmonary ECs, we proceeded to assess the impacts of MEOX1 and AIL on human pulmonary microvascular endothelial cells (HPMECs).

Overexpression of *MEOX1* in HPMECs (Fig. 5B) resulted in the upregulation of mesenchymal markers *ACTA2* and *vimentin* (*VIM*), along with the downregulation of endothelial markers *CD31* and *VE-cadherin* (*CDH5*) (Fig. 5C), indicating MEOX1 as a driver of EndMT in ECs. Then we applied TGF-β1 to HPMECs and investigated the role of AIL in EndMT. The qRT-PCR results revealed that AIL increased the mRNA level of *CD31* and decreased the expression of *ACTA2* and *VIM* compared to those in the TGF-β1-only group (Fig. 5D). Additionally, TGF-β1-treated HPMECs exhibited morphological changes associated with mesenchymal cells. High-content analysis based on fluorescence intensity indicated that AIL could restore the decrease of CD31 and VE-cadherin and inhibit the increase of α-SMA induced by TGF-β1 (Fig. 5E, F, Supporting Information Fig. S5A and S5B).

While normal ECs are quiescent and provide a tight endothelial barrier, fibrosis-associated ECs have high permeability, forming a leaky endothelial barrier[33]. The role of AIL in HPMECs permeability was determined by measuring FITC-albumin fluorescence intensity in the media in the lower chambers (Fig. 5G). We found that TGF-β1-treated HPMECs monolayers exhibited an increase in fluorescence intensity compared to the control group, and AIL decreased the fluorescence intensity after TGF-β1 stimulation (Fig. 5H), suggesting that AIL can reprogram fibrosis-associated ECs into normal lung ECs and restore the endothelial barrier in HPMECs after TGF-β1 stimulation.

At last, the effect of AIL on the migration of HPMECs was examined by scratch assays. TGF-β1-treated HPMECs showed increased migration compared with the control group, and AIL decreased TGF-β1-induced migration (Fig. 5I and J). These results were further confirmed by a transwell migration assay. As expected, cells in the lower transwell chamber in the group treated with both TGF-β1 and AIL significantly decreased compared to those in the TGF-β1-only group (Fig. S5C and S5D), suggesting that AIL suppressed the migration of HPMECs.

3.6. Ailanthone attenuated pulmonary fibrosis in mice induced by bleomycin

To assess the anti-fibrotic effects of AIL *in vivo*, we intratracheally administered bleomycin (BLM) to mice and then treated them with AIL. Preliminary experiments on normal mice, injected with varying concentrations of AIL every other day for two weeks, showed no abnormalities during the period in all tested doses (10, 5, 2.5, 1.25, and 0.625 mg/kg). Subsequent qRT-PCR analysis on these lung tissues revealed that AIL at doses of 5 and 10 mg/kg significantly reduced the expression of *Meox1* (Supporting Information Fig. S6A). Importantly, vital organs (heart, liver, spleen, and kidney) in AIL-treated mice (5 mg/kg) showed no changes compared to the saline-treated group (Fig. S6B). So we performed the subsequent experiments at a dose of 5 mg/kg AIL.

As illustrated in the experimental timeline (Fig. 6A), AIL treatment commenced on the second day after BLM injection and continued for 20 days, with JQ-1 used as a positive control. On Day 3, bronchoalveolar lavage fluid (BALF) and left lung samples were collected. H&E staining of left lung sections showed that the lung structure in the control and AIL groups appeared normal. In contrast, the BLM group exhibited evident alveolar inflammation, characterized by substantial infiltration and congestion of inflammatory cells (Fig. S6C). Alveolar inflammatory cell infiltration was still observable in the BLM + AIL and BLM + JQ-1 groups, but to a much lesser extent than in the BLM group (Fig. S6C and S6D). Similarly, AIL also significantly decreased the absolute cell numbers in BALF from the BLM + AIL group compared to those in the BLM group, implying a reduction in infiltrating inflammatory cells (Fig. S6E).

On Day 21, unconstrained whole-body plethysmography (WBP) was employed to evaluate lung function. AIL treatment significantly restored respiratory functions, evident in the increase of minute ventilation (MV), the reduction in inspiratory time (Ti), expiratory time (Te), and enhanced pause (Penh) compared to the BLM group (Fig. 6B and Fig. S6F). Subsequent assessments involved conventional detection methods for pulmonary fibrosis. AIL attenuated morphological changes in the lung and collagen deposition, as observed in H&E and Masson staining results (Fig. 6C–F). BLM treatment resulted in the upregulation of mesenchymal markers, specifically *Vim*, coupled with the downregulation of endothelial markers *Cd31* and *Cdh5* (Fig. 6G), indicating the occurrence of EndMT during BLM-induced pathogenesis. Conversely, AIL administration partially reversed the downregulation of *Cd31* and *Cdh5*, while also reducing the expression of *Vim* (Fig. 6G). This trend was further supported by immunofluorescence assays, which demonstrated that AIL suppressed the BLM-induced expression of α-SMA and restored the downregulation of Cd31 (Fig. S6G).

Figure 6 AIL attenuates Bleomycine-induced pulmonary fibrosis in mice. (A) Schematic diagram outlining the treatment strategy involving AIL or JQ-1 post bleomycin (BLM)-induced pulmonary fibrosis. (B) Enhanced pause (Penh) was assessed by WBP in each group on Day 21 after modeling; $n = 6$. (C) Representative images of HE staining of the lung section at Day 21 after BLM-induction, Scale bars: 300 μm. (D) Ashcroft score analysis of (C), $n = 6$ mice per group, 2 slices per mice. (E) Representative images of Masson's trichrome staining of the lung section on Day 21 after BLM-induction, Scale bars: 300 μm. (F) Collagen volume fraction analysis of (E); $n = 6$ mice per group, 2 slices per mice. (G) The mRNA levels of EndMT markers *Cd31*, *Cdh5* and *Vim* in lung tissues on Day 21 after BLM-induction were analyzed by qRT-PCR; $n = 3$. (H) The mRNA levels of *Meox1* and fibrotic markers *Acta2*, *Col1a1* and *Fn1* in lung tissues on Day 21 after BLM-induction were analyzed by qRT-PCR; $n = 9$. (I) The expression of Meox1, Collagen I, Fibronectin and Cd31 in lung tissues of mice was analyzed by Western blotting. (J) Quantitative analysis of protein expression in (I) was performed by ImageJ software; $n = 6$. (K) Quantitative hydroxyproline assay of the right lung in the groups as indicated; $n = 6$. Data are presented as mean ± SD; $^{\#}P < 0.05$, $^{\#\#}P < 0.01$, $^{\#\#\#}P < 0.001$, $^{\#\#\#\#}P < 0.0001$ by two-tailed Student's *t*-test; $^{*}P < 0.05$, $^{**}P < 0.01$, $^{****}P < 0.0001$ by one-way ANOVA followed by Tukey's *post hoc* test between indicated groups.

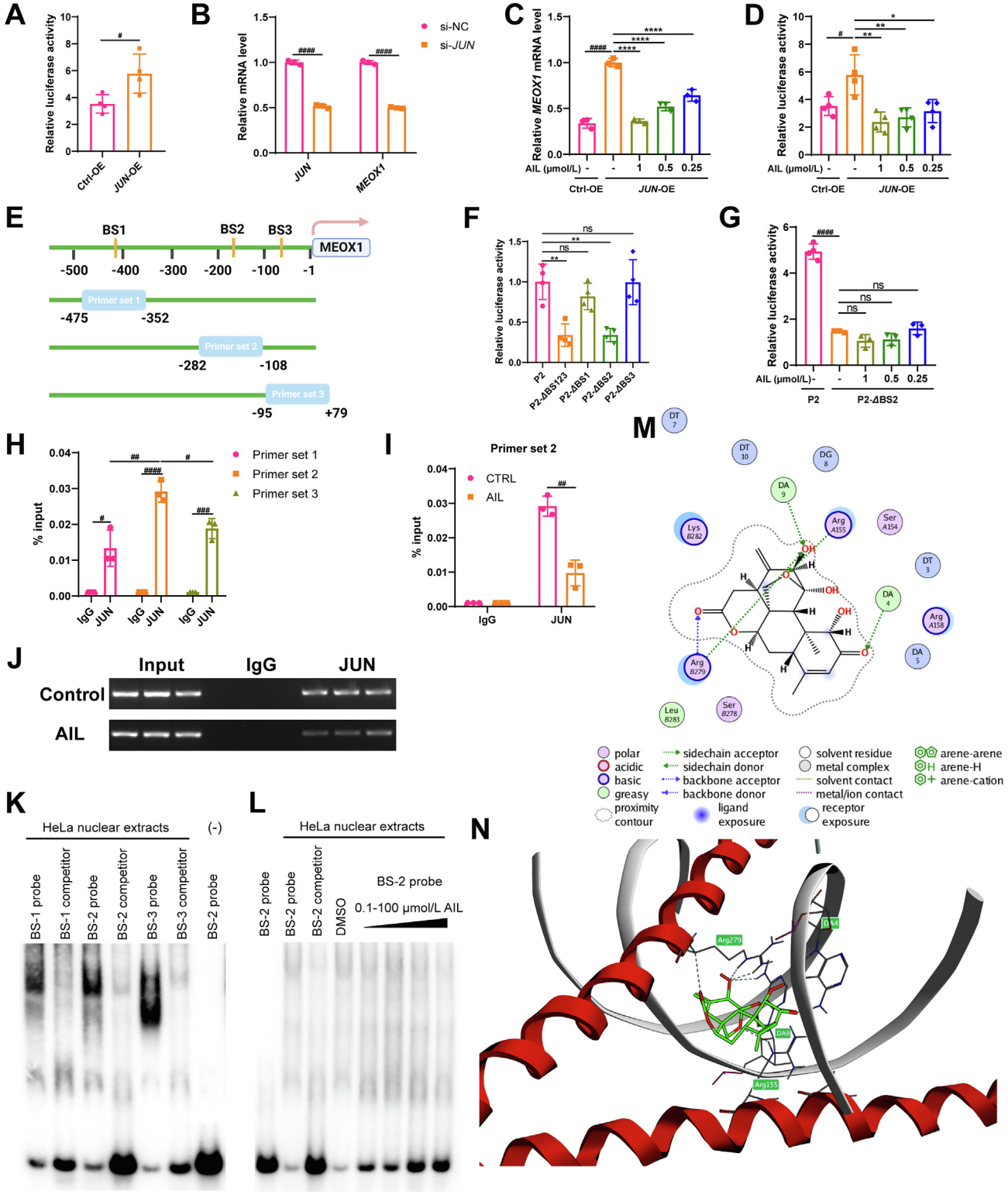

Figure 7 AIL suppressed MEOX1 transcription through JUN. (A) HeLa cells transfected with control vector or JUN-overexpressing plasmid were detected by dual luciferase reporter assays to reflect *MEOX1* promoter activity; $n = 4$. (B) HeLa cells were transfected with siRNA targeting JUN (si-*JUN*) or a scrambled control (si-NC) for 24 h, mRNA levels of JUN and MEOX1 was analyzed by qRT-PCR; $n = 3$. (C, D) HeLa cells transfected with control vector or *JUN*-overexpressing plasmid were treated with indicated concentrations of AIL for 24 h, and then the expression of *MEOX1* was analyzed by qRT-PCR (C) and the activity of *MEOX1* promoter was determined by dual luciferase reporter assay (D); $n = 3$. (E) Three potential JUN binding sites (BS) within *MEOX1* promoter were predicted by JASPAR. The relative location of BS sites in *MEOX1* gene and primers used in ChIP-qPCR to detect these sites were shown. (F) HeLa cells were transfected with P2-Fluc-Rluc (P2) or P2-ΔBS123, P2-ΔBS1, P2-ΔBS2, P2-ΔBS3 in which either one or all three BS sites were removed from P2, 48 h post-transfection dual luciferase reporter assays were

Given that ECM deposition is a key factor in pulmonary fibrosis, the expression of ECM components (Collagen I, Fibronectin) and the myofibroblast marker α-SMA were also investigated in lung tissues. AIL significantly attenuated the mRNA expression of *Meox1*, *Col1a1*, *Fn1*, and *Acta2* induced by BLM (Fig. 6F). Consistently, the protein levels of Meox1, Collagen I, Fibronectin and Cd31 were decreased after AIL treatment in BLM-induced mice (Fig. 6I and J). Furthermore, the amount of hydroxyproline, a specific amino acid in collagen, was reduced after AIL treatment (Fig. 6K). Meanwhile, AIL partially recovered the body weight of the BLM-mice and significantly improved the survival rate of mice with pulmonary fibrosis (Fig. S6H and S6I). In summary, these findings proved that AIL attenuated pulmonary fibrosis and restored respiratory functions in mice induced by bleomycin.

3.7. *Ailanthone suppressed MEOX1 expression by preventing JUN binds to MEOX1 promoter*

Our findings revealed a reduction in MEOX1 expression following AIL treatment, though the specific target of AIL remained unidentified. To discern the underlying mechanism governing AIL-mediated suppression of MEOX1, we employed the Similarity Ensemble Approach (SEA, https://sea.bkslab.org/)[34], a ligand-based prediction platform to refine the potential target for AIL. JUN, also known as c-Jun, a crucial component of transcription complex AP-1, was the only predicted target of AIL by SEA (Supporting Information Fig. S7A). Previous studies have established JUN as a common transcription factor activating various genes. Given this, we hypothesized that JUN might also activate MEOX1. To confirm our hypothesis, a MEOX1 luciferase reporter was constructed based on *MEOX1* P2 promoter. Luciferase assay results showed that overexpression of *JUN* significantly enhanced *MEOX1* promoter activity (Fig. 7A). Consistently, the overexpression of *JUN* in HeLa cells significantly increased endogenous *MEOX1* mRNA levels compared to the control group, while knocking down *JUN* revealed a reduction in *MEOX1* expression (Fig. 7B). More importantly, the overexpression of *JUN* partially rescued the downregulation of *MEOX1* caused by AIL as well as the reduction of P2 luciferase activity (Fig. 7C and D), suggesting the downregulation of MEOX1 under AIL treatment is mediated by JUN.

While we established that JUN binds to the *MEOX1* promoter, thereby inducing MEOX1 expression and activity, the specific binding sites for JUN within the promoter remained unclear. Using the online tool JASPAR (https://jaspar.elixir.no/), three potential JUN binding sites (BS) within the MEOX1 P2 promoter were predicted (Fig. 7E, Fig. S7B and S7C). To validate these specific sites, we conducted mutagenesis of the predicted sites, followed by dual luciferase reporter assays. The results showed that mutating all three BS sites significantly reduced the activity of *MEOX1* promoter (Fig. 7F). Notably, mutating only the second site (BS2: ATTAATCATC) had a significant impact, while mutation of the other two sites alone showed minimal impact (Fig. 7F). Crucially, the suppressive effect of AIL on *MEOX1* promoter activity was abolished when BS2 site was mutated (Fig. 7G). ChIP-qPCR analysis further confirmed that JUN directly binds to three sites within the *MEOX1* promoter, with the highest affinity observed at the BS2 site (Fig. 7H). More importantly, AIL treatment reduced the association of JUN with the *MEOX1* promoter (Fig. 7I and J). In line with the luciferase reporter assay and ChIP-qPCR results, electrophoretic mobility shift assay (EMSA) substantiated the direct binding of transcriptional factors to the three BS sites *in vitro* (Fig. 7K), with supper-shift EMSA confirming JUN's specific association with the BS2 site (Fig. S7D). Notably, AIL treatment dose-dependently disrupted the interaction between JUN and the BS2 site within *MEOX1* promoter (Fig. 7L).

We attempted to simulate the interaction of AIL with the JUN and MEOX1 DNA complex through molecular docking. The illustration of the AIL/AP-1/BS2 complex was generated, and residue interactions were analyzed using MOE 2022. AIL formed hydrogen bonds with Arg155 (on FOS) and Arg279 (on JUN) in the AP-1 complex, and simultaneously directly interact with DNA mainly through hydrogen bonds formed between AIL and dA4, dA9 on the BS2 sequence (sense: 5′-ATTAATCATC-3′, antisense: 3′-TAATTAGTAG-5′) (Fig. 7M and N). This result elucidated the mechanism by which AIL disrupts the binding of JUN to *MEOX1* promoter.

In summary, our data support the conclusion that AIL suppresses MEOX1 expression by preventing JUN binds to *MEOX1* promoter.

4. Discussion

IPF is a lethal disease with scarce therapeutic options. Currently, pirfenidone and nintedanib are the only small molecule drugs for IPF therapy[4]. While these drugs have demonstrated efficacy in slowing the decline of pulmonary function in IPF patients, nearly 20% of individuals are compelled to discontinue pirfenidone and nintedanib due to their severe side effects[5–7]. As a result, these drugs have been conditionally recommended by the FDA. Previous studies have highlighted the potential of targeting BET proteins to alleviate pulmonary fibrosis[19,20]. However, BET inhibitors suffer from non-selectivity and lack specificity, constraining their clinical utility in anti-fibrosis therapies[22].

To identify a clinically translatable target for pulmonary fibrosis, we pinpointed MEOX1, which exhibited significant upregulation in both idiopathic and interstitial pulmonary fibrosis patients, making it a potential candidate for anti-pulmonary

performed; $n = 4$. (G) HeLa cells were transfected with P2-ΔBS2, 24 h post-transfection, cells were treated with indicated concentrations of AIL for 24 h, activity of *MEOX1* promoter were detected by dual luciferase reporter assays; $n = 4$. (H) ChIP-qPCR assays for JUN binding ability to three BS sites in *MEOX1* promoter in HeLa cells. (I) ChIP-qPCR assays for JUN binding to the BS2 site (ATTAATCATC) in *MEOX1* promoter in HeLa cells with or without AIL treatment. (J) Agarose gel electrophoresis of the qPCR products in (I). (K) Biotin-labeled DNA probes containing BS1, 2 and 3 sequence within *MEOX1* promoter or 100-fold molar excess of unlabeled competitors (cold probes) were incubated with HeLa nuclear extracts, EMSA results was used to illustrate the specificity of the protein/DNA complexes. (L) Biotin-labeled DNA probe containing BS2 sequence was incubated with or without HeLa nuclear extracts, in the absence or presence of increasing concentrations of AIL. EMSA results was used to illustrate the effect of AIL on the association of protein and BS2. (M, N) The 2D and 3D residue interactions of the JUN/FOS/BS2 complex with AIL are depicted. The JUN/FOS/BS2 complex is illustrated as red and white ribbons with residues forming interaction shown as dashed lines. AIL is depicted in green. Data are presented as mean ± SD; $^{\#}P < 0.05$, $^{\#\#}P < 0.01$, $^{\#\#\#}P < 0.001$, $^{\#\#\#\#}P < 0.0001$ by two-tailed Student's *t*-test; $^{*}P < 0.05$, $^{**}P < 0.01$, $^{****}P < 0.0001$ by one-way ANOVA followed by Tukey's *post hoc* test between indicated groups.

fibrosis treatment. Previous studies found MEOX1 to be involved in organ development, affecting cell cycle, and inducing endothelial cell aging[35]. A recent report indicated a significant upregulation of MEOX1 in cardiac fibroblasts both in heart disease patients and a transverse aortic constriction (TAC)-induced mouse model. Treatment with JQ-1, a BET inhibitor, alleviated cardiac fibrosis by inhibiting MEOX1 expression[22]. Consistent with these findings, our study revealed that MEOX1 serves as a pivotal link connecting TGF-β1 with downstream profibrotic effectors in pulmonary fibrosis, and functions as the master switch in conversion of fibroblast-to-myofibroblast under TGF-β1 stimulation. Furthermore, we observed predominant expression of MEOX1 in lung endothelial cells, where elevated MEOX1 levels promoted EndMT during pulmonary fibrosis, representing another crucial mechanism by which MEOX1 contributes to the development of IPF. Consequently, inhibiting MEOX1 activity could effectively reduce the activation of two major cell sources contributing to IPF.

Transcription factors have long been deemed undruggable, attributed to their apparent structural disorders and the lack of well-defined binding pockets. Consequently, targeting MEOX1 poses a formidable challenge[23]. In this study, we implemented a HTS system based on the activity of *MEOX1* promoter and identified several small molecules within a natural compound library as potent suppressors of MEOX1. Natural products hold significant promise in drug discovery due to their advantageous pharmacological activities and low toxicity. The most promising candidate, Ailanthone (AIL), constitutes the primary active ingredient derived from the seeds and barks of *Ailanthus altissima*. AIL has been reported to exhibit a diverse range of pharmacological activities, including antibacterial, antiviral, anti-tuberculosis, antimalarial and anticancer effects[36]. A potent antitumor activity of AIL *in vivo* has been reported in hepatocellular carcinoma (HCC)[37], non-small cell lung cancer (NSCLC)[38] and castration-resistant prostate cancer (CRPC)[39]. In addition, AIL exhibits good solubility, pharmacokinetics, bioavailability, and has no inhibitory effect on cytochrome P450[39,40]. Nevertheless, its impact and mechanisms in anti-fibrosis have not been previously elucidated.

In this study, we have unveiled the potent therapeutic efficacy of AIL against pulmonary fibrosis for the first time. Specifically, AIL exhibits the capability to impede the fibroblast activation and EndMT stimulated by TGF-β1. Furthermore, it ameliorates BLM-induced pulmonary fibrosis in mice, underscoring its clinical potential as an anti-fibrotic agent. In contrast to JQ-1, AIL hinders MEOX1 transcription independently of BET proteins, thus circumventing the systemic effects associated with BET inhibition. Notably, while transcription factors are generally assumed to exert broad effects on diverse cellular functions, our scRNA-seq analysis reveal that MEOX1 is predominantly expressed in endothelial cells and fibroblasts. This restricted expression pattern of MEOX1 in specific cells presents an advantage over targeting ubiquitously expressed entities like BET proteins or TGF-β1. Additionally, the potential redundancy in functions between MEOX1 and its close homolog MEOX2 in endothelial cells might also serve to minimize side effects of AIL on MEOX1 suppression[41,42]. Recently, Wang et al.[43] suggested that MEOX1 inhibits the production of ROS and mitigates mitochondria-dependent apoptosis in doxorubicin-induced cardiotoxicity. Given the association of oxidative stress with the pathogenesis of IPF, further investigations into the role of MEOX1 in oxidative stress in alveolar epithelial cells are warranted. Additionally, considering MEOX1's involvement in mesodermal partitioning and somatic differentiation[44], MEOX1 inhibition might lead to developmental toxicity. This aspect should be considered when contemplating MEOX1 as a clinically translatable target for IPF, particularly in cases involving pregnancy.

Furthermore, our investigation into the specific target of AIL has unveiled the mechanism underlying MEOX1 activation in the progression of pulmonary fibrosis. The TGF-β1/SMAD pathway is a classical shared pathway implicated in numerous fibrotic diseases[45–47]. Previous reports indicated that SMAD binds to the promoter and enhancer of MEOX1, representing a subsequent step in the fibrosis regulation through the TGF-β1/SMAD pathway[22]. Our findings, on the other hand, revealed that the transcription factor JUN binds to the *MEOX1* promoter, enhancing its transcription. Crucially, AIL exhibited a dose-dependent capability to counteract the activation of MEOX1 by JUN. Additionally, AIL hindered the expression of MEOX1 by preventing the binding of JUN/FOS to the ATTAATCATC motif on the *MEOX1* promoter, ultimately leading to a reduction in pulmonary fibrosis. Notably, our study corroborated that SMAD can collaborate with JUN/FOS to activate the transcription of downstream effectors and mediators in response to TGF-β1[48,49], uncovering a novel mechanism of MEOX1 activation in a JUN-dependent manner (Fig. 8).

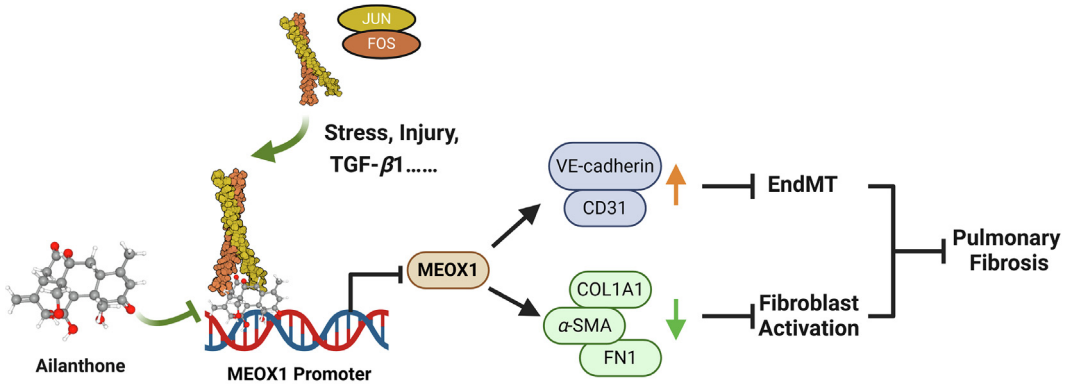

Figure 8 Cartoon depicts how Ailanthone ameliorates pulmonary fibrosis by suppressing JUN-dependent MEOX1 activation. Injury and/or stress induce the recruitment of the AP-1 transcription complex to the *MEOX1* gene through binding of JUN to the ATTAATCATC motif on the *MEOX1* promoter. This enhances MEOX1 expression, subsequently causing the activation of fibroblasts and EndMT of endothelial cells, ultimately leading to pulmonary fibrosis. Ailanthone functions as a potent MEOX1 suppressor by disrupting the interaction between JUN and the *MEOX1* promoter. This disruption inhibits MEOX1 expression and activity, resulting in the amelioration of pulmonary fibrosis both *in vitro* and *in vivo*.

While prior studies have suggested that targeting AP-1 can alleviate fibrosis, the intricate mechanism underlying this process remains to be fully elucidated[47,50−55]. Our study contributes a rationale for understanding the role of AP-1 in fibrosis, particularly by facilitating MEOX1 activation through JUN binding to the *MEOX1* promoter and subsequently augmenting the expression of downstream fibrosis-related genes. Both TGF-β1 and AP-1 play broad and diverse roles in various physiological processes. Consequently, directly targeting them may disrupt essential functions, potentially resulting in undesirable side effects. In contrast, MEOX1 stands out as a more specific target for the treatment of pulmonary fibrosis.

In a recent study, it was reported that AIL degrades JUN protein in melanoma cells[56]. However, in our investigation, we observed that AIL did not exert a significant impact on the protein level of JUN (Supporting Information Fig. S8A). This discrepancy may be attributed to cell heterogeneity. Meanwhile, AIL has shown the ability to degrade the androgen receptor (AR)[39]. Interestingly, we observed a substantial upregulation of AR in pulmonary fibrosis patients, although the elevated level was not as pronounced as that of MEOX1 (Fig. S8B). Currently, the role of the AR in fibrosis is not well-established. These findings suggest the possibility of additional mechanisms through which AIL reduces pulmonary fibrosis, warranting further investigation.

5. Conclusions

Our study establishes MEOX1 as a pivotal link connecting TGF-β1 with downstream profibrotic effectors in pulmonary fibrosis and identifies Ailanthone (AIL) as a potent suppressor of MEOX1 by disrupting the interaction between JUN and the *MEOX1* promoter. These findings pinpoint MEOX1 as a cell-specific and clinically translatable target in pulmonary fibrosis, and implicate the great clinical potential of AIL in the treatment of various fibrotic diseases.

Acknowledgments

We are grateful for financial support from National Key R&D Program of China (2022YFE0209700), the National Natural Science Foundation of China (82070406, 82000080, and 82304486), and Guangdong Provincial Drug Administration Science and Technology Innovation Program (2023ZDZ05, 2022ZDZ10, China). This work was also supported by a funding from the Department of Science and Technology of Guangdong to AS (2024A1515010574, China).

Author contributions

Lixin Zhao: Conceptualization, Data curation, Formal analysis, Investigation, Writing − original draft, Writing − review & editing. Yuguang Zhu: Data curation, Formal analysis, Investigation, Methodology, Validation. Hua Tao: Data curation, Formal analysis, Investigation, Validation. Xiying Chen: Data curation, Investigation, Validation. Feng Yin: Data curation, Investigation. Yingyi Zhang: Data curation, Investigation. Jianfeng Qin: Data curation, Investigation. Yongyin Huang: Data curation. Bikun Cai: Data curation. Yonghao Lin: Data curation. Jiaxiang Wu: Data curation. Yu Zhang: Formal analysis, Funding acquisition. Lu Liang: Formal analysis, Funding acquisition. Ao Shen: Conceptualization, Formal analysis, Funding acquisition, Investigation, Supervision, Writing − original draft, Writing − review & editing. Xi-Yong Yu: Conceptualization, Formal analysis, Funding acquisition, Project administration, Supervision, Writing − review & editing.

Conflicts of interest

The authors declare no conflicts of interest exist.

Appendix A. Supporting information

Supporting information to this article can be found online at https://doi.org/10.1016/j.apsb.2024.04.013.

References

1. Wynn TA, Ramalingam TR. Mechanisms of fibrosis: therapeutic translation for fibrotic disease. *Nat Med* 2012;**18**:1028−40.
2. Henderson NC, Rieder F, Wynn TA. Fibrosis: from mechanisms to medicines. *Nature* 2020;**587**:555−66.
3. Raghu G, Remy-Jardin M, Richeldi L, Thomson CC, Inoue Y, Johkoh T, et al. Idiopathic pulmonary fibrosis (an update) and progressive pulmonary fibrosis in adults: an official ATS/ERS/JRS/ALAT clinical practice guideline. *Am J Respir Crit Care Med* 2022;**205**:e18−47.
4. Tzilas V, Tzouvelekis A, Ryu JH, Bouros D. 2022 update on clinical practice guidelines for idiopathic pulmonary fibrosis and progressive pulmonary fibrosis. *Lancet Respir Med* 2022;**10**:729−31.
5. King TJ, Bradford WZ, Castro-Bernardini S, Fagan EA, Glaspole I, Glassberg MK, et al. A phase 3 trial of pirfenidone in patients with idiopathic pulmonary fibrosis. *N Engl J Med* 2014;**370**:2083−92.
6. Cottin V, Maher T. Long-term clinical and real-world experience with pirfenidone in the treatment of idiopathic pulmonary fibrosis. *Eur Respir Rev* 2015;**24**:58−64.
7. Kolb M, Raghu G, Wells AU, Behr J, Richeldi L, Schinzel B, et al. Nintedanib plus sildenafil in patients with idiopathic pulmonary fibrosis. *N Engl J Med* 2018;**379**:1722−31.
8. Moss BJ, Ryter SW, Rosas IO. Pathogenic mechanisms underlying idiopathic pulmonary fibrosis. *Annu Rev Pathol* 2022;**17**:515−46.
9. Gaikwad AV, Eapen MS, Mcalinden KD, Chia C, Larby J, Myers S, et al. Endothelial to mesenchymal transition (EndMT) and vascular remodeling in pulmonary hypertension and idiopathic pulmonary fibrosis. *Expert Rev Respir Med* 2020;**14**:1027−43.
10. May J, Mitchell JA, Jenkins RG. Beyond epithelial damage: vascular and endothelial contributions to idiopathic pulmonary fibrosis. *J Clin Invest* 2023;**133**:e172058.
11. Spagnolo P, Kropski JA, Jones MG, Lee JS, Rossi G, Karampitsakos T, et al. Idiopathic pulmonary fibrosis: disease mechanisms and drug development. *Pharmacol Ther* 2021;**222**:107798.
12. Massague J, Sheppard D. TGF-β signaling in health and disease. *Cell* 2023;**186**:4007−37.
13. Liu G, Philp AM, Corte T, Travis MA, Schilter H, Hansbro NG, et al. Therapeutic targets in lung tissue remodelling and fibrosis. *Pharmacol Ther* 2021;**225**:107839.
14. Katsuno Y, Derynck R. Epithelial plasticity, epithelial-mesenchymal transition, and the TGF-beta family. *Dev Cell* 2021;**56**:726−46.
15. Zhang H, Huang X, Liu K, Tang J, He L, Pu W, et al. Fibroblasts in an endocardial fibroelastosis disease model mainly originate from mesenchymal derivatives of epicardium. *Cell Res* 2017;**27**:1157−77.
16. Lachapelle P, Li M, Douglass J, Stewart A. Safer approaches to therapeutic modulation of TGF-β signaling for respiratory disease. *Pharmacol Ther* 2018;**187**:98−113.
17. Stratton MS, Bagchi RA, Felisbino MB, Hirsch RA, Smith HE, Riching AS, et al. Dynamic chromatin targeting of BRD4 stimulates cardiac fibroblast activation. *Circ Res* 2019;**125**:662−77.
18. He Z, Jiao H, An Q, Zhang X, Zengyangzong D, Xu J, et al. Discovery of novel 4-phenylquinazoline-based BRD4 inhibitors for cardiac fibrosis. *Acta Pharm Sin B* 2022;**12**:291−307.

19. Wang J, Zhou F, Li Z, Mei H, Wang Y, Ma H, et al. Pharmacological targeting of BET proteins attenuates radiation-induced lung fibrosis. *Sci Rep* 2018;**8**:998.
20. Kaneshita S, Kida T, Yoshioka M, Nishioka K, Raje M, Sakashita A, et al. CG223, a novel BET inhibitor, exerts TGF-β1-mediated anti-fibrotic effects in a murine model of bleomycin-induced pulmonary fibrosis. *Pulm Pharmacol Ther* 2021;**70**:102057.
21. Ding N, Hah N, Yu RT, Sherman MH, Benner C, Leblanc M, et al. BRD4 is a novel therapeutic target for liver fibrosis. *Proc Natl Acad Sci U S A* 2015;**112**:15713−8.
22. Alexanian M, Przytycki PF, Micheletti R, Padmanabhan A, Ye L, Travers JG, et al. A transcriptional switch governs fibroblast activation in heart disease. *Nature* 2021;**595**:438−43.
23. Schumacher D, Peisker F, Kramann R. MEOX1: a novel druggable target that orchestrates the activation of fibroblasts in cardiac fibrosis. *Signal Transduct Target Ther* 2021;**6**:440.
24. Sun J, Jin T, Su W, Guo Y, Niu Z, Guo J, et al. The long non-coding RNA PFI protects against pulmonary fibrosis by interacting with splicing regulator SRSF1. *Cell Death Differ* 2021;**28**:2916−30.
25. Charan J, Kantharia ND. How to calculate sample size in animal studies?. *J Pharmacol Pharmacother* 2013;**4**:303−6.
26. Ashcroft T, Simpson JM, Timbrell V. Simple method of estimating severity of pulmonary fibrosis on a numerical scale. *J Clin Pathol* 1988;**41**:467−70.
27. Jaffar J, Wong M, Fishbein GA, Alhamdoosh M, Mcmillan L, Gamell-Fulla C, et al. Matrix metalloproteinase-7 is increased in lung bases but not apices in idiopathic pulmonary fibrosis. *ERJ Open Res* 2022;**8**: 00191-2022.
28. Henley MJ, Koehler AN. Advances in targeting 'undruggable' transcription factors with small molecules. *Nat Rev Drug Discov* 2021;**20**: 669−88.
29. Kirilenko P, He G, Mankoo BS, Mallo M, Jones R, Bobola N. Transient activation of meox1 is an early component of the gene regulatory network downstream of hoxa2. *Mol Cell Biol* 2011;**31**:1301−8.
30. Ghonim MA, Boyd DF, Flerlage T, Thomas PG. Pulmonary inflammation and fibroblast immunoregulation: from bench to bedside. *J Clin Invest* 2023;**133**:e170499.
31. Habermann AC, Gutierrez AJ, Bui LT, Yahn SL, Winters NI, Calvi CL, et al. Single-cell RNA sequencing reveals profibrotic roles of distinct epithelial and mesenchymal lineages in pulmonary fibrosis. *Sci Adv* 2020;**6**:eaba1972.
32. Reyfman PA, Walter JM, Joshi N, Anekalla KR, Mcquattie-Pimentel AC, Chiu S, et al. Single-cell transcriptomic analysis of human lung provides insights into the pathobiology of pulmonary fibrosis. *Am J Respir Crit Care Med* 2019;**199**:1517−36.
33. Martin M, Zhang J, Miao Y, He M, Kang J, Huang HY, et al. Role of endothelial cells in pulmonary fibrosis *via* SREBP2 activation. *JCI Insight* 2021;**6**:e125635.
34. Keiser MJ, Roth BL, Armbruster BN, Ernsberger P, Irwin JJ, Shoichet BK. Relating protein pharmacology by ligand chemistry. *Nat Biotechnol* 2007;**25**:197−206.
35. Zeng G, Liu X, Su X, Wang Y, Liu B, Zhou H, et al. The role of MEOX1 in non-neoplastic and neoplastic diseases. *Biomed Pharmacother* 2023;**158**:114068.
36. Ding H, Yu X, Hang C, Gao K, Lao X, Jia Y, et al. Ailanthone: a novel potential drug for treating human cancer. *Oncol Lett* 2020;**20**: 1489−503.
37. Zhuo Z, Hu J, Yang X, Chen M, Lei X, Deng L, et al. Ailanthone inhibits Huh7 cancer cell growth *via* cell cycle arrest and apoptosis *in vitro* and *in vivo*. *Sci Rep* 2015;**5**:16185.
38. Ni Z, Yao C, Zhu X, Gong C, Xu Z, Wang L, et al. Ailanthone inhibits non-small cell lung cancer cell growth through repressing DNA replication *via* downregulating RPA1. *Br J Cancer* 2017;**117**:1621−30.
39. He Y, Peng S, Wang J, Chen H, Cong X, Chen A, et al. Ailanthone targets p23 to overcome MDV3100 resistance in castration-resistant prostate cancer. *Nat Commun* 2016;**7**:13122.
40. Chen A, Qin X, Lu J, Yi Z, Liu M, Wang X. Development of a validated LC−MS/MS method for the determination of Ailanthone in rat plasma with application to pharmacokinetic study. *J Pharm Biomed Anal* 2015;**102**:514−8.
41. Douville JM, Cheung DY, Herbert KL, Moffatt T, Wigle JT. Mechanisms of MEOX1 and MEOX2 regulation of the cyclin dependent kinase inhibitors p21 and p16 in vascular endothelial cells. *PLoS One* 2011;**6**:e29099.
42. Mankoo BS, Skuntz S, Harrigan I, Grigorieva E, Candia A, Wright CV, et al. The concerted action of Meox homeobox genes is required upstream of genetic pathways essential for the formation, patterning and differentiation of somites. *Development* 2003;**130**:4655−64.
43. Wang W, Fang Q, Zhang Z, Wang D, Wu L, Wang Y. PPARα ameliorates doxorubicin-induced cardiotoxicity by reducing mitochondria-dependent apoptosis *via* regulating MEOX1. *Front Pharmacol* 2020; **11**:528267.
44. Candia AF, Hu J, Crosby J, Lalley PA, Noden D, Nadeau JH, et al. *Mox-1* and *Mox-2* define a novel homeobox gene subfamily and are differentially expressed during early mesodermal patterning in mouse embryos. *Development* 1992;**116**:1123−36.
45. Song Y, Wei J, Li R, Fu R, Han P, Wang H, et al. Tyrosine kinase receptor B attenuates liver fibrosis by inhibiting TGF-β/SMAD signaling. *Hepatology* 2023;**78**:1433−47.
46. He X, Cheng R, Huang C, Takahashi Y, Yang Y, Benyajati S, et al. A novel role of LRP5 in tubulointerstitial fibrosis through activating TGF-β/Smad signaling. *Signal Transduct Target Ther* 2020;**5**:45.
47. Wygrecka M, Zakrzewicz D, Taborski B, Didiasova M, Kwapiszewska G, Preissner KT, et al. TGF-β1 induces tissue factor expression in human lung fibroblasts in a PI3K/JNK/Akt-dependent and AP-1-dependent manner. *Am J Respir Cell Mol Biol* 2012;**47**:614−27.
48. Zhang Y, Feng XH, Derynck R. Smad3 and Smad4 cooperate with c-Jun/c-Fos to mediate TGF-β-induced transcription. *Nature* 1998;**394**: 909−13.
49. Zheng X, Qi C, Zhang S, Fang Y, Ning W. TGF-β1 induces Fstl1 *via* the Smad3-c-Jun pathway in lung fibroblasts. *Am J Physiol Lung Cell Mol Physiol* 2017;**313**:L240−51.
50. Schulien I, Hockenjos B, Schmitt-Graeff A, Perdekamp MG, Follo M, Thimme R, et al. The transcription factor c-Jun/AP-1 promotes liver fibrosis during non-alcoholic steatohepatitis by regulating osteopontin expression. *Cell Death Differ* 2019;**26**:1688−99.
51. Lorenzen JM, Schauerte C, Hubner A, Kolling M, Martino F, Scherf K, et al. Osteopontin is indispensible for AP1-mediated angiotensin II-related mir-21 transcription during cardiac fibrosis. *Eur Heart J* 2015;**36**:2184−96.
52. Eferl R, Hasselblatt P, Rath M, Popper H, Zenz R, Komnenovic V, et al. Development of pulmonary fibrosis through a pathway involving the transcription factor Fra-2/AP-1. *Proc Natl Acad Sci U S A* 2008; **105**:10525−30.
53. Wang J, He F, Chen L, Li Q, Jin S, Zheng H, et al. Resveratrol inhibits pulmonary fibrosis by regulating miR-21 through MAPK/AP-1 pathways. *Biomed Pharmacother* 2018;**105**:37−44.
54. Wernig G, Chen SY, Cui L, Van Neste C, Tsai JM, Kambham N, et al. Unifying mechanism for different fibrotic diseases. *Proc Natl Acad Sci U S A* 2017;**114**:4757−62.
55. Cui L, Chen SY, Lerbs T, Lee JW, Domizi P, Gordon S, et al. Activation of Jun in fibroblasts promotes pro-fibrotic programme and modulates protective immunity. *Nat Commun* 2020;**11**:2795.
56. Yu P, Wei H, Li K, Zhu S, Li J, Chen C, et al. The traditional Chinese medicine monomer ailanthone improves the therapeutic efficacy of anti-PD-L1 in melanoma cells by targeting c-Jun. *J Exp Clin Cancer Res* 2022;**41**:346.